Multi-Objective Optimal Design of Lithium-Ion Battery Cells

By

Yao Hong

A thesis submitted in partial fulfillment
of the requirements for the degree of
Master of Science in Engineering
(Industrial and Systems Engineering)
in the University of Michigan–Dearborn
2016

Master's Thesis Committee:

Associate Professor Cheol Lee, Chair
Assistant Professor Jian Hu
Associate Professor Yung-wen Liu

Acknowledgements

I wish to express a deep sense of gratitude to Dr. Cheol Lee for his inspiration, encouragement and timely guidance to this research.

Table of Contents

List of Figures

List of Tables

List of Appendices

Abstract

Lithium ion battery has been considered as a promising candidate to improve the current fossil fuels based energy economy. Massive efforts have been put in the optimal design of lithium ion batteries with the assistance of simulation models. But to our knowledge, the application of multi-objective optimization in this process has not been well discussed. The purpose of this thesis is to study the multi-objective optimization problems that could be applied on the optimal design of lithium ion batteries with the assistance of simulation models.

A two-objective problem is firstly constructed with the performance measures of energy per unit separator area for the discharge rate of 0.5C and the mass per unit separator area. The reaction zone model and genetic algorithm are employed to solve this problem qualitatively. The resulted Pareto front comes out to be a concave curve in the 2D plane of the two performance measures. Three case studies are guided to illustrate the advantages and applications of employing the multi-objective optimization in the design process.

A DAE based simulation model is then employed and tuned to have a satisfying fit to the charge and discharge curves for the cycling rates up to 4C. With the assistance of this precise simulation model, the properties of the Pareto front of the two-objective optimization is then validated quantitatively.

A three-objective optimization problem with the objectives of energy performance of 0.25C and 4C discharge and mass performance is then constructed to extend the analysis of applications of multi-objective oriented studies in lithium-ion battery designs. The problem is quantitatively resolved with the assistance of the DAE based simulation model and genetic

algorithm. The Pareto front comes out to be a curved surface in the 3D space of the three objectives. The properties of the Pareto front are expected to offer perspectives and references to product designs in the industry.

Chapter 1. Introduction

Lithium Ion batteries have been considered as one of the most promising energy storage devices for improving the current fuel economy. A well designed cell which has better performance in some perspectives is obviously preferred in many applications.

The purpose of this research is to explore the application of multi-objective optimization in Lithium-ion battery cell design. This chapter offers the background and motivation of this research. The objectives of this research is listed in Section 1.2. After that, a literature review is given in Section 1.3. Section 1.4 will presents approaches used for the research and the thesis layout.

1.1 Background and Motivation

It is widely believed that most of the global environmental issues are closely related with the current energy economy based on fossil fuels. This situation is required to be changed urgently. The general agreement is that the share of the sustainable energy sources needs to greatly increase [1][2]. However, many sustainable energy sources, such as wind energy and solar power, rely heavily on environmental conditions which vary day to day. Therefore, these energy sources tend to be intermittent and their daily energy production might be difficult to control. To compensate for the limitations of sustainable sources, high-performance energy storage systems are required so that the excess produced energy during “good times” can be well stored for future use in “bad times”.

It is often stated that the CO_2 issues and the air pollutions in large urban areas may be solved only by replacing internal combustion engine (ICE) cars with zero emission vehicles, i.e. electric vehicles (EVs) or controlled emission vehicles, i.e. hybrid electric vehicles (HEVs) and plug-in hybrid electric vehicles (PHEVs). These vehicles also require high performance energy-storage devices so that they can provide a proper power performance and an adequate daily operation range.

Among the current candidates, one of the most promising energy storage devices for the aforementioned applications is the Lithium Ion battery. A Ragon plot is often used for performance comparisons of various energy-storage devices [3]. It is a plot where both specific energy and specific power are shown, such that people can have a good understanding of both energy performance and power performance for energy storage devices. As it can be seen in Figure 1-1, the fuel cells are very good at specific energy, but for high power applications, their power performance is not adequate. In contrast, the capacitors have a very good power density, while their energy density is not high enough for energy storage purposes.

The conventional electrochemical batteries, although performing relatively poor in high power applications, are well capable in energy storage for low rate applications. Therefore, they are be considered as one of the most promising candidates for compensating for the intermittent characteristic of sustainable sources [2]. As shown in Figure 1-1, among all the electrochemical batteries, Lithium-ion batteries have best performance in terms of both energy density and power density. Thus, in recent years, more and more attentions have been paid to the lithium-ion batteries due to their high specific energy, high efficiency and long life.

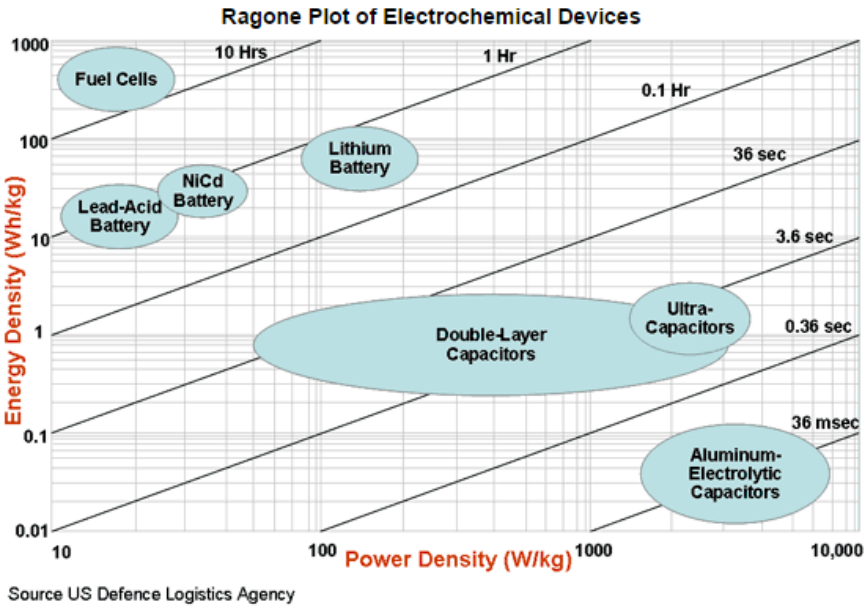

Figure 1-1 Ragon Plot for Electrochemical Devices

The optimal design of Lithium-Ion batteries has been a popular topic and heavily discussed by researchers in recent years. These researches, however, are mostly focused on single objective optimization while an actual product design process needs to consider multiple performance measurements.

The motivation of this research is to explore the application of multi-objective optimization to the lithium-ion battery designs and its advantages when compared to the single objective oriented studies. The results of this study are expected to become valuable references for design of experiments (DOE) and product design in the industry.

1.2 Research Objectives

The purpose of this research is to study a novel methodology for optimal design of Lithium Ion battery cells by using electrochemical simulation models and multi-objective optimization as tools. The objectives of the research include:

- Construct a multi-objective optimization problem for optimal design of lithium-ion battery cells, which is widely applicable to multiple real world problems.
- Study simulation models that are proper for qualitative and quantitative analysis respectively, discuss the tuning and validation process for electrochemical simulation models.
- Explore the characteristics of the Pareto front of constructed multi-objective optimization problem and illustrate the capability of the solutions for the constructed problem.
- Quantitatively obtain the Pareto optimal set for a LiFePO4-Graphite Li-Ion battery with a well-tuned electrochemical simulation model. Use the results to validate the characteristics of the Pareto front discussed, illustrate the application of the solutions.
- Discuss the relationship between the outcomes of this research and the industry.

1.3 Literature Reviews

This section reviews the application of simulation models and optimization problems for battery optimal designs.

Regarding the simulation models for lithium-ion battery charging and discharging activities, Shriram Santhanagopalan[4] reviewed the three mostly commonly used types of simulation models in his work, which are P2D models, SP models and PP models. The pseudo 2D model (P2D model) is the most computational expensive. In this model, the solid phase is assumed to be comprised of identical spherical particles of a predetermined size and diffusion in the radial direction is assumed to be the predominant mode of transport. The solution phase concentration and potential were assumed to vary in only one direction (from positive electrode to negative electrode), thus the discharging or charging became a 2D process based on

movements of ions and electrons. The P2D model is often considered as a complete model because of its high accuracy. Some researchers even use the predictions of the P2D model as a reference to validate the other simulation models. The single particle model (SP) and the porous electrode model with the polynomial approximation (PP) model are two approximate models. In a SP model, each electrode is represented by a single spherical particle whose area is equivalent to that of the active area of the solid phase in the porous electrode. This assumption massively reduced the scale of the P2D model because only one spherical particle needs to be considered for each electrode. Thus, the computation costs of SP model is much lower than the P2D model. However, It was shown that SP model is not capable to hold a good precision when the discharge rate is higher than 1C although it is more efficient [4, 16]. Weilin Luo [5] extended the SP model so that it can be applied to higher discharge rates up to 4C with a sufficient accuracy. SP model is a great candidate for real time battery management systems because of its high efficiency, but to study the mechanics or optimal design of lithium-ion batteries, a PP model is more appropriate. A PP model does not assume each electrode has only one single particle and holds all the assumptions used in the P2D model so that it is not as computationally efficient as the SP model. However, by employing mathematically simpler polynomial approximations in the model, its computational cost is still greatly reduced compared with the P2D model. Besides, as the computing power of PC has been improving in a fast pace, the PP model can already be efficient enough for optimization purposes. Beyond these three most commonly used simulation models, another simple simulation model, which is called the reaction zone model, was introduced in [6]. This model, however, seems only valid for some qualitative analysis because of its simplicity.

Studies on the optimization of lithium-ion battery cell designs are reported in the literature [6-13]. However, most of these efforts are single-objective oriented. In [6] and [7], the

specific energy of battery cells was optimized by changing the porosity and thickness of cathode, while in [8], the influence of cathode porosity and thickness on the electronic conductivity was studied and ionic conductivity was maximized the specific energy with these two design variables as well. In [9], the ohimic drop across the cell was minimized by modifying the distribution profile of porosity in the electrodes. The minimum usable capacity of cell for a range of discharge rates was optimized in [10] by changing the distribution of porosity and particle size. All these single-objective based studies were targeted at identifying one optimal design which gives the best value for the performance measure selected by the authors.

The specific energy and specific power are both employed as objectives in [11]. The result of the optimization was a Pareto front which consists of a set of non-dominated designs. These designs were the trade-offs between the two objective functions and the designers were allowed to pick the most proper one from the Pareto front based on their target application. However, one of the design variable considered in this paper was the discharge rate, which should be determined by the target application and not appropriate to be considered as a design variable. Also, the construction of proper optimization problems for lithium-ion battery optimal designs was not well discussed by the authors.

The most significant difference between multi-objective optimization problems (MO) and single-objective optimization problems (SO) is that instead of identifying a single solution to minimize or maximize an objective function, the target of MO is to determine a set of trade-offs between multiple contradictory objective functions [15][17][29]. This set is referred as Pareto optimal set or Pareto front.

A design is defined to be dominated by another if it is no better in all objectives, and worse in at least one objective [11]. The designs included in the Pareto front are those which are

not dominated by any other designs. In concept, a design is said to be Pareto optimal if no other designs can be better in all objectives than this one.

Genetic algorithm (GA) is one of the commonly used heuristic algorithms for solving optimization problems. To solve an SO, GA repeatedly generate generations by "mixing" the genes of randomly selecting pairs of individuals from the parent generations (crossover) and partially alter the genes of the individuals (mutation). By imitating the process of natural selection, the individuals with better fitness values will be maintained in each step as the new parent generation and used to generate the next child generation. With the mutation operation, the diversity of the individuals is enhanced. Because of the crossover operation, the more "adapted" genes in a generation are combined. Over successive generations, the population is likely to "evolve" to an optimal solution [20]. To solve an MO, although crossover and mutation are still used to generating each generation, but instead of identifying the single optimal individual, the algorithm identifies a set of non-dominated solutions. The non-dominated solutions get closer to the Pareto-optimal set from generation to generation and an estimated Pareto front can be obtained after a number of generations. More details about GA can be found in [18] and [19].

1.4 Research Approach and Organization of the Thesis

As stated in Section 1.3, many researches have been using simulation models to study the properties of lithium-ion batteries, some of them also considered the simulation models as the tool for optimal designs because of the relatively low costs of simulation compared with physical design of experiments.

Most of these studies were single-objective oriented. Only a few researches employed multi-objective optimization problems as the tool for lithium-ion battery optimal designs. However, to our knowledge, how to construct a multi-object optimization problem for the lithium-ion cell designs whose solutions can be applied for different target applications has not been well discussed.

Two simulation models are employed in this thesis to discuss the multi-objective optimization problems for optimal designs of lithium-ion batteries. The first model studied is the reaction zone model. Introductions to this model can be found in Section 2.1 and Appendix I. although it is an overly simplified simulation model, it can still reflect the changes of energy performance of the cells when a couple of design variables are changed in a qualitative manner. The second model employed is a DAE-based PP model, while requires more computations than the reaction zone model does, it is quantitatively more accurate when predicting the charge and discharge curves at multiple cycling rates. Because of the properties of each model, the reaction zone model is used for qualitative discussion, the DAE based simulation model is used for quantitative analysis.

A two-objective optimization problem for lithium-ion battery optimal designs is constructed in Chapter 2. The reaction zone model is implemented with MATLAB. With the assistance of the global optimization toolbox, the genetic algorithm is used to solve the two-objective optimization problem. The Pareto front of the problem is revealed and the properties are discussed. Using three case studies, the wide applicability of the constructed problem is illustrated. The advantages of applying multi-objective optimization in product designs are demonstrated by the analysis performed in this chapter. However, due to the simplicity of the reaction zone model, the discussions in Chapter 2 are limited to qualitative ones.

To enhance the analysis capability to allow the quantitative analysis, a DAE based PP model is introduced and tuned in Chapter 3. A process of tuning parameter selection is illustrated in Section 3.2, a tuning problem is constructed and solved in Section 3.3. The tuned simulation model shows good agreement with the experiment data for cycling rates up to 4C and can be used to quantitatively estimate the Pareto front of multi-objective optimization problems constructed for lithium-ion battery designs. It is believed that the similar process can be applied for the tuning of other simulation models.

Chapter 4 illustrates the quantitative analysis for the application of multi-objective optimization problems in the lithium-ion battery design domain. Section 4.1 validates the results and analysis in Chapter 2 by using the quantitatively precise DAE-based simulation model to solve the two-objective optimization problem constructed before. A three-objective optimization problem is constructed in Section 4.2 and solved in Section 4.3 with the tuned model. The obtained Pareto front for the three-objective problem is a curved surface. The properties and applications of this surface is discussed in Section 4.4.

Chapter 5 is a summary chapter. The results and discussions of former chapters will be summarized in Section 5.1. The limitations of the current project and the future efforts will be discussed in Section 5.2.

Chapter 2. A Two-Objective Optimization Problem and the Qualitative Analysis for the Problem with A Reaction Zone Model

In this chapter, a simple reaction zone simulation model is firstly introduced in Section 2.1. This model is not as precise as a PP model or SP model is, but it elegantly shows the trend of responses when the values of some design variables are changed, thus can be a very proper tool for a qualitative analysis.

A two-objective design problem is constructed in Section 2.2 and will be referred as the base problem in the thesis. This problem considers energy generated during discharging and the mass of the battery cell for unit separator areas as objectives.

By analyzing the problem and the reaction zone model adopted, the anticipated shape of Pareto front is also discussed in Section 2.3. By using a genetic algorithm implemented by MATLAB and the introduced reaction zone model, the solutions for the base problem are obtained in Section 2.3, which is able to validate the anticipated Pareto front.

Then three case studies are discussed in Section 2.4. These cases show that the solution to the base problem can be applied in different design problems, which means the base problem is widely applicable for different design purposes and do not need to be solved repeatedly

Section 2.5 gives a discussion about the advantages of applying multi-objective optimization for the optimal design of lithium-ion battery cell. Also, some discussion about

qualitative analysis and quantitative solutions for the design problem is issued in this section as well.

2.1 Reaction Zone Model

This thesis adopted a reaction zone model for the first stage of analysis. Although simplified, a reaction zone model if capable of offering some perspectives of how the design variables will influence the performance of a battery and thus is considered as a proper tool for a qualitative analysis in the thesis. Figure 2-1 shows a schema for the reaction zone model [29].

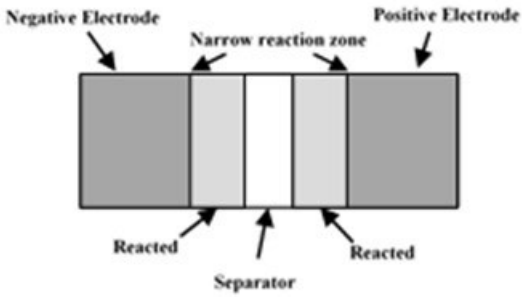

Figure 2-1 Schema of a Reaction Zone Model

In a reaction zone model, both positive and negative electrodes can be divided into the reacted and the unreacted regions. Between these two regions are the narrow reaction zones. All the chemical reactions are assumed to happen in the reaction zones. When discharging, the ionic current must flow from the reaction zone in negative electrode, through the porous reacted region in negative electrode, separator, the porous reacted region in positive electrode up to the reaction zone in positive electrode. The two reaction zones, during the discharging, will move from the separator to the current collectors since the active materials will be used up slowly [29].

For different unit separator area, the distribution of active materials, the diffusion and the chemical reactions are assumed to be the same. Therefore, the problem can be simplified so that all the modeling could focus on a unit separator area. In the reaction zone model, the energy per unit separator area is calculated by Equation (2-1)

$$E = \left(U - \frac{L_s}{\kappa_s} i\right) i t_d - \frac{i^3 t_d^2}{2\kappa_+(1-\epsilon_+)q_+} - \frac{i^3 t_d^2}{2\kappa_-(1-\epsilon_-)q_-} \quad (2\text{-}1)$$

where U is the open circuit voltage, L_s is the thickness of separator, i is the discharge current density, t_d is the discharge time, κ_s, κ_+ and κ_- are the effective conductivities of the electrolyte in separator, positive, and negative electrodes respectively, ϵ_+ and ϵ_- are the porosity of positive and negative electrodes respectively, q_+ and q_- are the capacity density of active materials in positive and negative electrodes respectively. See the Appendix I for more details about the reaction zone model [29].

The mass per unit separator area of the cell can be obtained by Equation (2-2).

$$M = M_r + M_s + M_+ + M_- \quad (2\text{-}2)$$

where M_r, M_s, M_+, and M_- are the mass of remaining parts, separator, positive electrode and negative electrode in a unit separator area domain respectively. For separator, positive and negative electrodes, each of their unit area mass can be obtained by Equation (2-3)

$$M_i = [\rho_i(1-\epsilon_i) + \rho_e \epsilon_i] L_i \quad (2\text{-}3)$$

where ρ_i is the density of solid phase in electrode i (can be s, $+$ or -), ϵ_i is the porosity, ρ_e is the density of electrolyte and L_i is the thickness [29].

The mass of the remaining parts is assumed to be obtained with Equation (2-4). It consists of two parts, one is assumed to be proportional to the mass of separator, and the other is the mass of the aluminum current collectors.

$$M_r = bM_s + M_{collector} \quad (2\text{-}4)$$

where b is the assumed proportion, M_s is the unit area mass of separator and $M_{collector}$ is the unit area mass of current collectors [29].

The parameters used in the model are summarized in Table 2-1.

Table 2-1 Summary of Design Variables and Parameters in Model

Design Variables	Symbols	Optimization Range
Cathode thickness	L_+	$0\sim500\ \mu m$
Cathode porosity	ϵ_+	$0\sim0.99$
Parameters	**Symbols**	**Value Used**
Cathode active material density $(LiFePO_4)$[r]	ρ_+	$3.6\ g/cm^3$
Anode active material density $(graphite)$[r]	ρ_-	$2.27\ g/cm^3$
Separator solid phase density[r]	ρ_s	$0.9\ g/cm^3$
Electrolyte density[r]	ρ_e	$1.2\ g/cm^3$
Current collectors density $(Aluminum)$[r]	$\rho_{collector}$	$2.7\ g/cm^3$
Anode porosity[r]	ϵ_-	0.33
Separator porosity[r]	ϵ_s	0.55
Open-circuit voltage[r]	U	$3.3\ V$
Cut-off voltage[r]	V_C	$2.5\ V$
Cathode solids capacity density	q_+	$2190.24\ C/cm^3$
Anode solids capacity density	q_-	$3023.64\ C/cm^3$
Inherent electrolyte conductivity[r]	κ_0	$0.005\ S/cm$
Capacity ratio between electrodes[a]	r	1.1
Discharge time[a]	t_d	$2\ hrs$
Mass ratio between remaining parts and separator[a] (except for collector)[a]	b	2
Total current collector thickness[r]	--	$55\ \mu m$
a. Assumed r. Ref [7]		

More details of reaction zone model can be found in Appendix I, as building a simulation model is not the purpose of the thesis, these contents are not included in the main chapters.

2.2 Construction of a Two-Objective Design Problem (Base Problem)

In former studies, several performance measures [6][7][8][9][10][11][12][13] of Li-ion batteries were adopted. However, the most common one of them can be specific energy for a fixed discharge time. Specific energy is defined as energy per unit mass, thus it simultaneously reflects two aspects of battery performance, the energy and the mass. But since only the ratio of

energy and mass is the objective while doing optimization, these studies were only able to find a single optimal design, which offers none flexibility when trade-off between energy and mass is required [29].

This chapter would also consider these two aspects at the same time, but not combined as a single objective (specific energy). Energy performance and mass performance are considered separately as two objectives and thus makes the problem a multi-objective optimization. Thus, more flexibility will be obtained when we need trade-off between energy and mass. To simplify the analysis, both objectives are measured in a unit separator area domain [29].

As Venkat Srinivasan [7] stated, changes to the design of the positive electrode would have more significant impact on performance than changes to the negative electrode do. This chapter therefore will focus on the design of positive electrode [29].

Thickness and Porosity of positive electrode are considered as design variables, while the porosity of negative electrode is assumed to be constant and the thickness of it is modified to keep the capacity ratio of two electrodes fixed ($\frac{C_-}{C_+}$ is usually larger than 1) [7]. The objectives for the problem are given as follows.

$$Maximize. E = f_1(L_+, \epsilon_+) \tag{2-5}$$

$$Minmize. M = f_2(L_+, \epsilon_+) \tag{2-6}$$

where E is the energy per unit separator area delivered by the cell for a predetermined discharging time, t_d, M is the mass per unit separator area of the cell. L_+ is the thickness of positive electrode, and ϵ_+ is the porosity of positive electrode [29].

The constraints of the design variables include

$$0 < \varepsilon_+ < 1 \tag{2-7}$$

$$0 \leq L_+ \leq L_{max} \tag{2-8}$$

where L_{max} is the largest allowed thickness for the positive electrode [29].

The problem illustrated in this section will be referred as the "base problem" in the thesis. The base problem will be solved in this chapter, and it's showed that the solutions to this base problem are powerful enough to solve several different design problems in practice [29].

2.3 Qualitative Solutions to the Two-Objective Design Problem

As the base problem is a multi-objective optimization problem, the result is expected to be a Pareto front which consists of a set of optimal solutions. The shape of this front can offer product designers general perspectives about how changes in design variables would influence the performance of lithium-ion batteries, thus guides them to do appropriate design of experiments and product designs [29].

As can be inferred, by employing a reaction zone model, the optimal Pareto front for the base problem would be a concave curve as shown in Figure 2-2. The slope of a straight line connecting any point on the front and the origin of coordinates corresponds to the specific energy of the corresponding designs, which is equal to the energy per unit area divided by the mass per unit area [29].

Since the parameters for the separator are assumed to be constant, when the thickness of positive electrode is zero, the cell will still have some mass because of the existence of separator and the remaining parts (current collectors for example). The Pareto front, therefore, would start at a non-zero point on the Mass (per unit area) axis. Once some active materials and electrolyte are added into the cell, some energy could be delivered although the unit area mass is increased a bit. This means the specific energy has increased from zero to some positive magnitude. At first, as the marginal return of unit area energy because of the increase of another unit area mass

would be large enough, the specific energy will stay increasing. However, as the marginal return is expected to reduce when the unit area mass becomes greater, after some point, the specific energy would start to decrease. More theoretical analysis about the expected shape of Pareto front can be found in Appendix II [29].

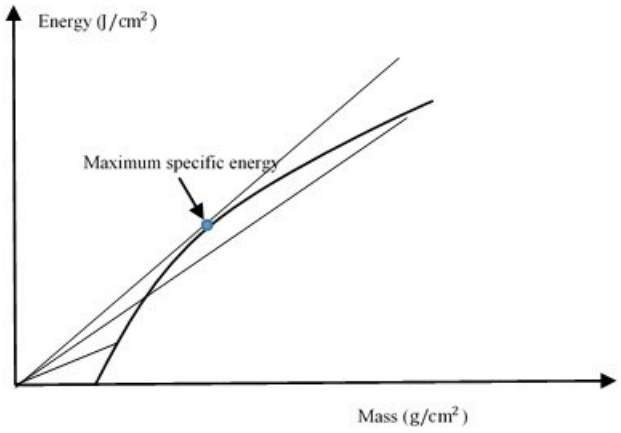

Figure 2-2 Expected Shape Pareto Front of the Base Problem

To validate the expected shape of this Pareto front, a simulation model based on reaction zone model was built with MATLAB and the genetic algorithm was implemented to solve the optimization problem [29].

To implement the GA, the function of gamultiobj in Global Optimization Toolbox was used. This function uses a controlled elitist genetic algorithm (a variant of NSGA-II) [21]. The options used for this function can be set with the function of gaoptimset [21]. The default values usually work well, but to better estimate the Pareto-optimal set in this case, the default population size, 50 is too small. Thus, the population size was set as 225, and the other options are kept at their default values in this study. The results of the optimization validated the expected shape of Pareto front, see Figure 2-3 [29].

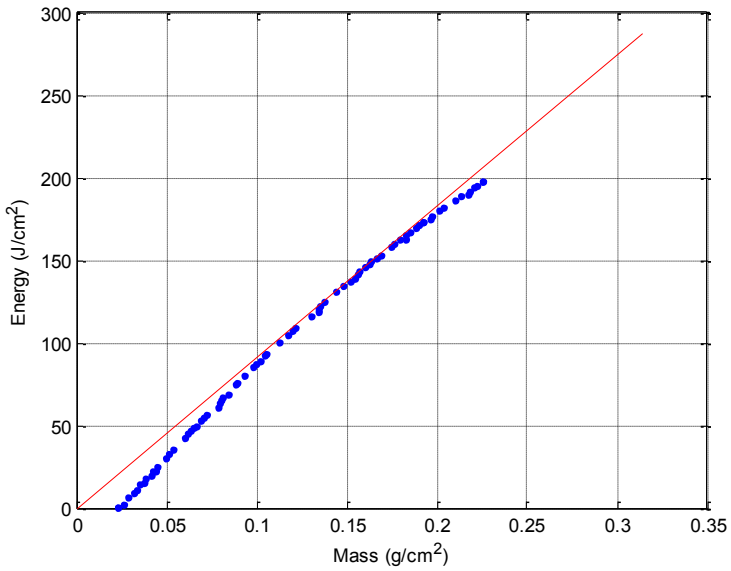

Figure 2-3 Pareto Front of Simulation Model

As can be shown in the Figure 2-2 and Figure 2-3, the former efforts of determining the design with the largest specific energy will only give people a particular solution included in the optimal solution set, while the whole front offer the designers much more flexibility since many more available options are included in the optimal set which may have a lower specific energy, but would be a lighter or smaller design [29].

In this thesis, a smaller design means smaller separator area required for target energy since the size of large energy cells will be mainly determined by the area, not the thickness. This is because that the thickness of cell electrodes will be at a level of micrometers, when the target energy is large, the area of separator will be at a much larger magnitude. Although making thicker electrodes also helps increasing the energy capacity of cells, the effect is limited. Appendix III gives a more detailed analysis for this problem [29].

In the next Section, the use of this Pareto front will be discussed with three design case studies.

2.4 Case Studies

Three case studies involving multi-objective optimization are carried out in this section. The first case adopts the objectives of maximizing the energy and minimizing mass and indicates that this is the same with maximizing specific energy. The second case adopts the objectives of minimizing separator area and cell mass while reaching a target energy requirement. This case makes sense when there is a target application. The third case adopts the objectives of maximizing unit area energy and specific energy. This case can be the reality when there isn't a target application. It is demonstrated here that the solutions to the base problem in the Analysis Section are capable of handling all the three cases. Discussions about the limitations of this study and some possible future works are illustrated in section 2.5 [29].

Case Study 1: Maximize Total Energy and Minimize Total Mass

In portable or EV applications, a general problem is to design a high-capacity battery of a light weight. This corresponds to an optimization problem of maximizing total energy and minimizing the total mass simultaneously [29].

The difference between this case and the base problem is that the separator area now becomes a design variable which will influence both objective functions [29].

$$Maximize.Energy = E \times A \tag{2-9}$$

$$Minimize.Mass = M \times A \tag{2-10}$$

The results of this problem could be illustrated in Figure 2-4. Figure 2-4(a) shows the Pareto front for the base problem in section 2.2, while Figure 2-4(b), which includes separator area as an additional design variable, is composed with a set of similar curves. The difference between these curves is due to the change of the area of separator. However, when total energy is

maximized and total mass is minimized simultaneously, the Pareto front will be a straight line which could envelop all the set of curves, which is the red dashed line in Figure 2-4(b) [29].

This result indicates the same optimal design with the commonly used objective of maximizing the specific energy, which is point A1 in Figure 2-4(a) [29].

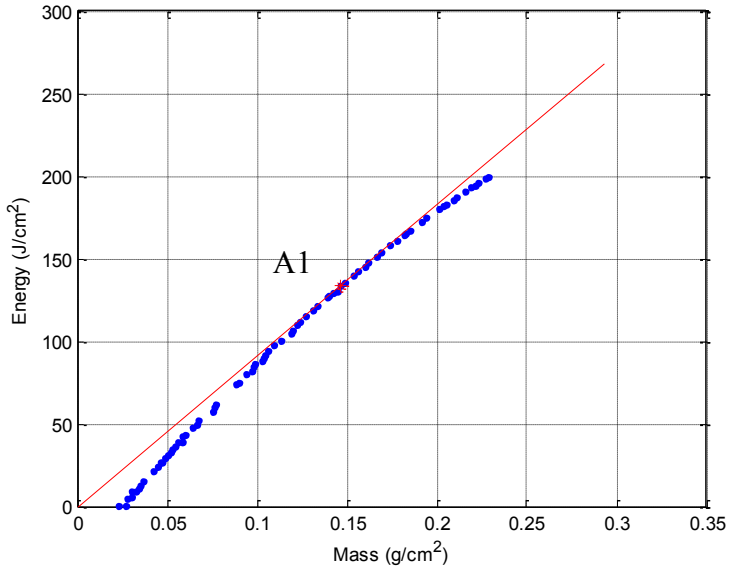

(a)Pareto front for a unit area

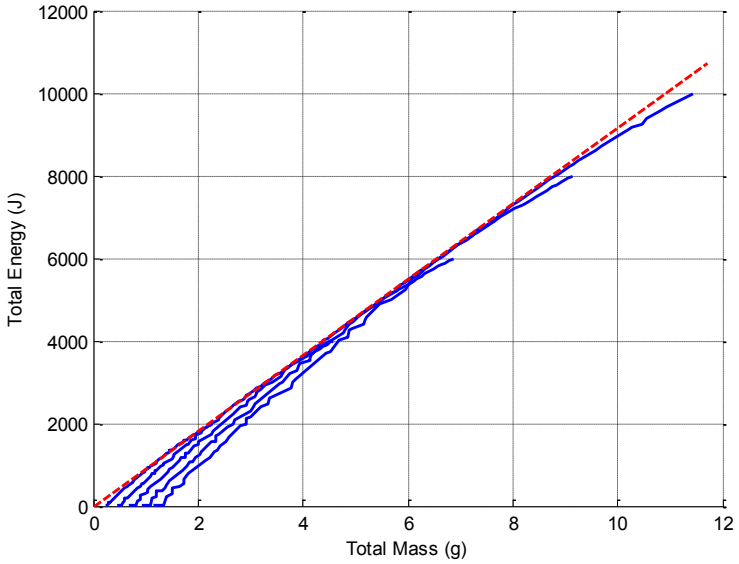

(b)Pareto fronts for different area

Figure 2-4 The Relationship Between Base Problem and Design for Maximized Specific Energy

Case Study 2: Minimize Area and Mass for a Target Energy

This case concerns applications for which the battery designers have a predetermined target energy requirement with a fixed discharge time. Under this circumstance, the total energy required becomes a constraint, and minimizing the weight and the size of a cell become the objectives. The size of a cell was measured by the separator area, as stated in the Section 2.3, separator area is dominating in the cell size [29].

Thus, compared with the base problem, a new multi-objective optimization can be formulated as follows.

$$Minimize. A = \frac{TE}{E} \tag{2-11}$$

$$Minimize. Mass = M \times A \tag{2-12}$$

where TE is the target energy, E and M are unit area energy and unit area mass respectively [29].

The solutions of this multi-objective optimization, however, could be directly obtained from the Pareto front for the base problem and no additional optimization needs to be guided [29].

Figure 2-5(a) shows the Pareto front of the base problem, while Figure 2-5(b) shows the transformed Pareto front for this case from the solutions of the base problem (for an arbitrary determined target energy 1,000J). Point A1 in Figure 2-5(a) corresponds to the design which would maximize the specific energy, hence minimizing the mass when the required energy is given. Thus, it corresponds to the point A2 in Figure 2-5(b). The point B1 on the other hand, has the largest unit area energy according to the base problem, thus will give the smallest separator area in this case (B2) [29].

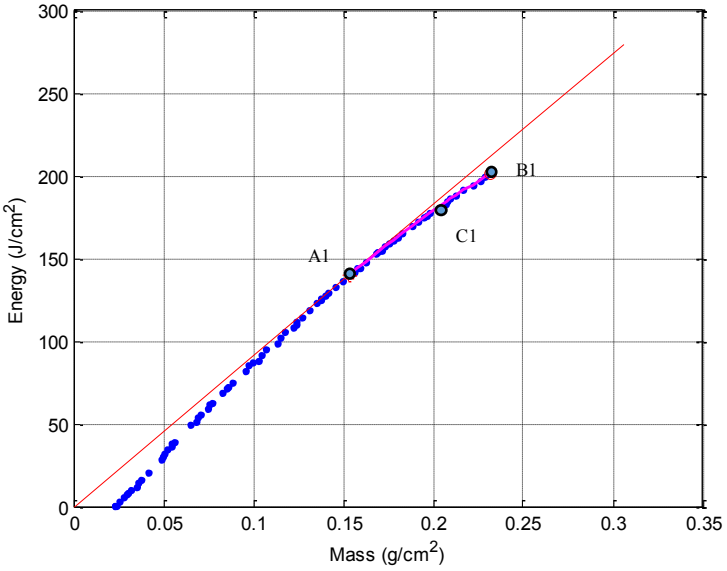

(a) Pareto front of the base problem

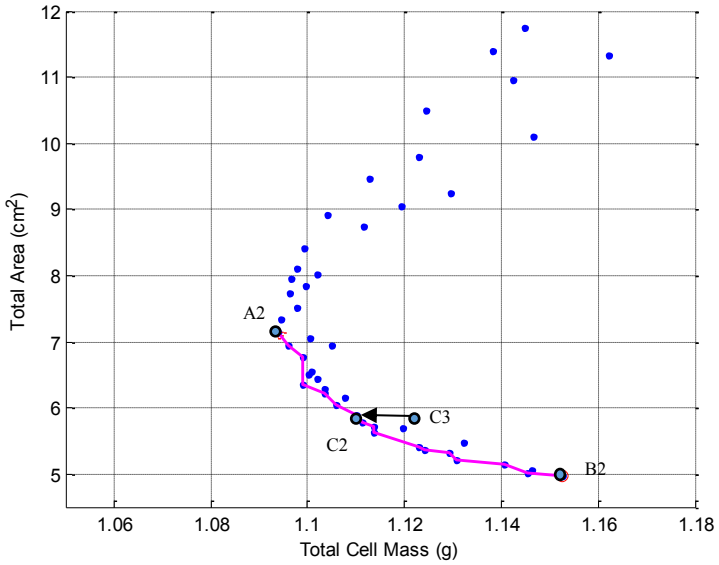

(b) Pareto front of Case 2

Figure 2-5 The Relationship between Base Problem and Design with a Target Application

It's easy to prove that a point lies between A1 and B1 and along the Pareto front in the base problem, say point C1, would correspond to a point along the Pareto font in Figure 2-5(b) as well. If we assume in Figure 2-5(b), the corresponding design for C1 is C3 rather than C2, then

we can always find another better design which could reduce the Mass while keeping the separator area fixed. This also means in the base problem, we can identify a design which could increase the unit area energy but keep the unit area mass fixed compared with C1. If so, the point C1 in Figure 2-5(a) no longer belongs to the Pareto optimal set, which is not consistent with the assumption. Thus, C1 has to correspond to a point belongs to the Pareto front in Figure 2-5(b), say C2 [29].

So, the solid magenta parts in the two plots are corresponding with each other. The dashed parts (lower parts for Figure 2-5(a) and upper parts of Figure 2-5(b)) are corresponding with each other as well. But as we are now identifying the Pareto front in this case, considering the dashed parts do not belong to the Pareto front for this case, no interests will be given to these parts. Note that the points in Figure 2-5(b) are not strictly composing a smooth curve. This is due to the computation limitation in GA optimization [29].

It can be observed that when having an energy target for a discharge time, designers do not have to guide another optimization to obtain the lightest or the smallest design, or a trade-off. Once the base problem is solved, the results of the base problem are enough to handle the problem put forward in this case [29].

Case Study 3: Maximize Unit Area Energy and Specific Energy

In some cases, the designers may not have an energy target. The designers, however, know the expected discharge time and always want to design lighter and smaller cell. A lighter cell is often corresponding to a greater specific energy, while a smaller one corresponding to greater unit area energy. Thus, another multi-objective optimization problem can be formulated as follows

$$Maximize.\, E = f_1(L_+, \epsilon_+) \tag{2-13}$$

$$Maximize.\, SE = \frac{E}{M} \tag{2-14}$$

where E and M are unit area energy and unit area mass respectively, and SE is the specific energy for the discharge time [29].

Figure 2-6 is an illustration for the transformed results of this case from the solutions to the base problem. Still, it's easy to infer that A1, B1 and C1 in Figure 2-6(a) are corresponding to A2, B2 and C2 in Figure 2-6(b) respectively through the logic illustrated in Case 2 [29].

Thus, the Pareto front for this problem can be directly obtained from the solutions of the base problem as well. Under the context of multi-objective optimization, only the solid magenta parts (rights parts of Figure 2-6(a) and (b)) in the plots will be important. In Figure 2-6, point A1 and point A2 still correspond to the design with the largest specific energy. Still, because of computation limitation in GA optimization, the points in Figure 2-6(b) failed to compose a smooth curve [29].

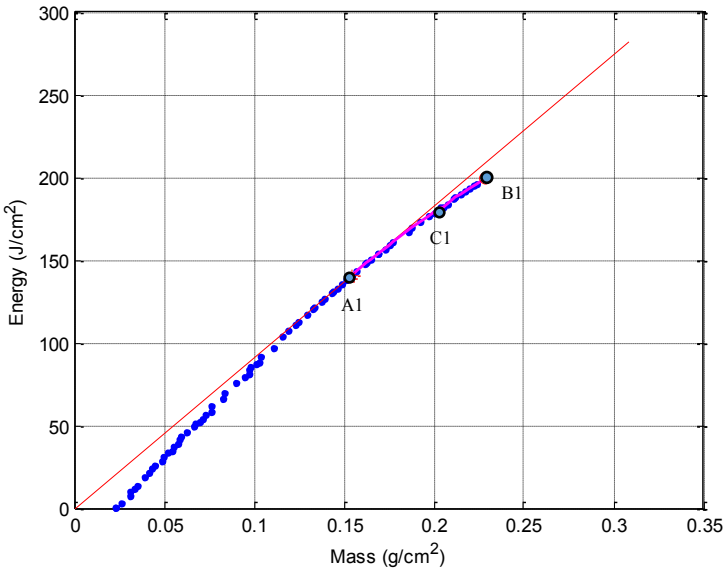

(a) Pareto front of the base problem

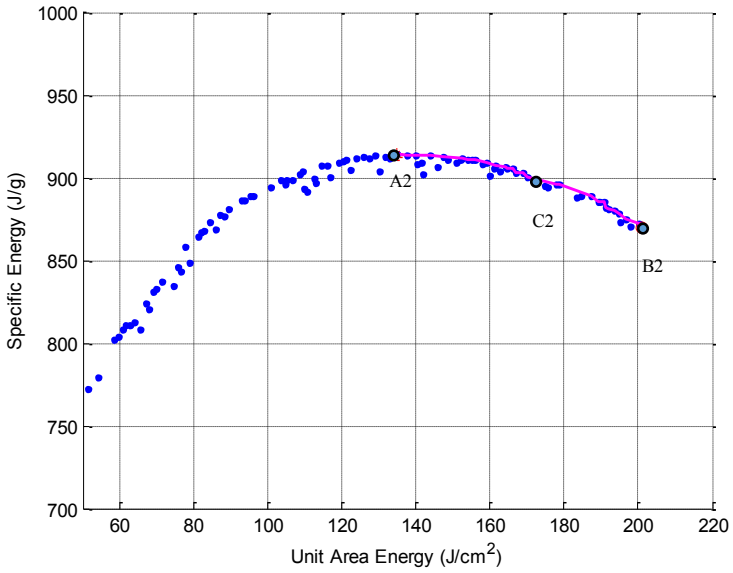

(b) Pareto front of Case 3

Figure 2-6 The Relationship Between Base Problem and Design without a Target Application

2.5 Discussion

Typical single objective oriented design process only offers one optimal design based on the objective function set by designers. This is usually not the case in real word production designs as a real design has to tradeoff between multiple contradictory performance measures so that a design which fits the target applications can be identified.

This chapter described the process of constructing a multi-objective optimization problem for lithium-ion battery designs and discussed its capability to be applied in multiple design cases. As can be seen, compared with the typical single objective oriented methodologies, this methodology allows the designers to pick up the most appropriate designs from the generated optimal Pareto set and thus is flexible to different kinds of applications. Although the cost of solving a multi-objective optimization problem is way much higher than single-objective problems, the way we set up the base problem makes it applicable for multiple different design

targets designers may encounter in the industry. As the solutions to the base problem are capable in multiple design cases, the multi-objective optimization problem does not need to be solved repeatedly when facing different problems, which compensate the high costs of solving such kinds of problems.

In this chapter, only two design variables are considered, which are thickness and porosity of positive electrode due to the simplicity of reaction zone model. Researchers have been interested in other independent variables in the Li-ion battery design as well [7][8][9][10][11][12][16]. However, the chapter demonstrates the benefits of multi-objective optimization in lithium-ion batteries design [29].

Conceptually, if more design variables such as particle size are included in the optimization, the authors believe a similar shape for the Pareto front of the base problem will be obtained and here give the reasons [29].

When the electrode thickness is zero, no energy would be delivered by the cell, and the mass will be equal to the mass of separator and the remaining parts, so the Pareto front will start from a none-zero point on the axis of mass per unit area. Once some changes are made to the design, the specific energy of this cell would be increased from zero to some positive value. So after the beginning point, an increasing trend on the Pareto front for specific energy can be expected for some range of design variables. However, when the constraints for design variables become binding and the contradiction between objectives becomes significant, the marginal gain of energy due to the increase in the mass would be reduced. Thus, most likely, after some point on the Pareto Front, the Specific Energy would start to fall [29].

If more design variables are considered, more degrees of freedom are given to the optimization. So a higher Pareto Front compared to the case where we have only two design

variables can be expected. But the shape of the Pareto front is expected to stay according to the discussion above [29].

This chapter only focused on the battery performance on the aspect of energy measures, the high power performance was not included. The expected output if a high power performance is added to the base problem as another objective to maximize is that the Pareto front becomes a surface in the three-dimensional space rather than a curve [29]. Also, because of the simplicity and limitations of the reaction zone model, the discussion in this chapter is limited in a qualitative manner.

We expect to have more design variables and the high power performance measure included in the problem, and we wish the problem can be discussed quantitatively with accurate solutions and confident conclusions. These procedures acquire a more complex and accurate model (e.g. PP model). In chapter 3, a more advanced simulation model will be adopted and tuned. With the tuned model, the high power performance will be added into the base problem as another objective and this problem will be discussed and solved quantitatively in chapter 4.

Chapter 3. Tuning A DAE Based Simulation Model for $LiFePO_4$-Graphite Batteries

Chapter 2 already described the shape of Pareto front of the constructed multi-objective optimization problem. Although qualitatively, the application of multi-objective optimization in Lithium-Ion Battery cell designs and its advantages have been well presented with such a discussion. However, it is not capable enough for a reaction zone model to give some quantitative results.

To acquire quantitative results for this problem, a more advanced, accurate simulation model has to be adopted, tuned and validated so that we can be confident that the responses of the tuned simulation model will be close to the reality according to the change of design variables.

This chapter gives a simple introduction to a DAE based simulation model for LiFePO4-Graphite Li-Ion Batteries. The model is tuned to fit the experimental data of charging and discharging curves for multiple charge/discharge rates. To do so, another optimization problem is constructed with the objective of minimizing the sum of squared residuals between the model predictions and experimental charging/discharging curves. Section 3.2 illustrated the tuning parameters in this optimization problem. Genetic Algorithm is used to find the optimal tuning parameters in Section 3.3, by validating the simulation with multiple discharge/charge curves, the model is considered a good fit for further quantitative analysis in this thesis.

3.1 A Compact Differential-Algebraic Equations Model for LiFePO4-Graphite Li-Ion Batteries

In a Pseudo two-dimensional model (P2D) [4], the solid phase is usually assumed to comprise of identical spherical particles of a predetermined size and the diffusion in the radial direction is assumed to be predominant mode of transport. The concentration of solution phase and the potentials were usually assumed to vary only in the 'x' coordinate, which is shown in Figure 3-1.

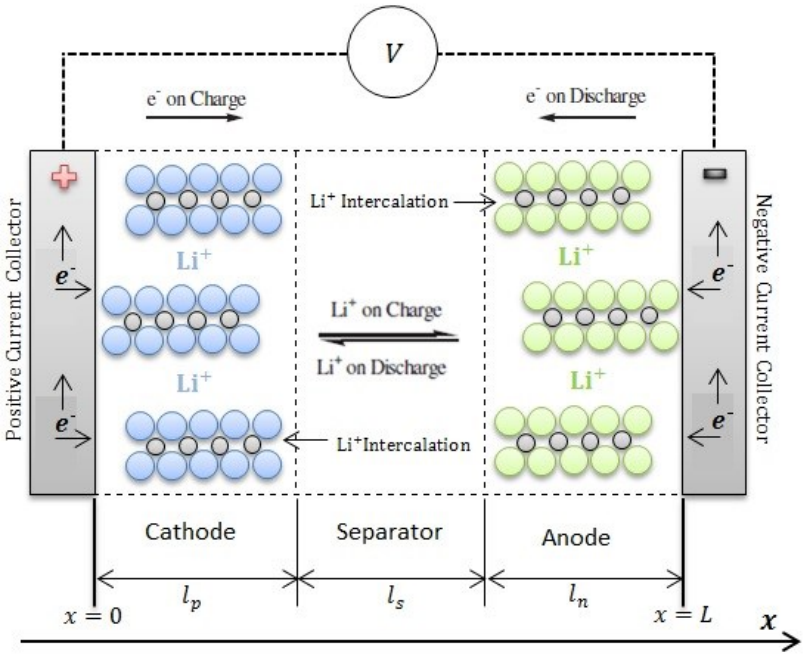

Figure 3-1 Schema of a P2D Electrochemical Model of Li-Ion Battery Error! Reference source not found.

The governing equations of a P2D model include solid-phase concentrations, electrolyte concentration, charge conservation in solid-phase and charge conservation in electrolyte. P2D model is often considered as a complete model to compare with the other approximate

methodologies in researches [4]. But a P2D model is not efficient enough for optimization and real time battery management purposes because of its high complexity.

This project adopted polynomial representations for the electrolyte concentration and solid-phase concentrations to derive a DAE system, which make the model a porous electrode model with the polynomial approximation (PP). Subramanian [23] discovered that the number of dependent variables can be made small by representing the pore-wall flux by a polynomial approximation as well, which is also adopted in the model of this project. To explain the measurable change in open circuit potentials during charging and discharging for $LiFePO_4$ batteries, the hysteresis phenomenon is also considered in the model.

More details of the simulation model can be found in [30]. As the purpose of this thesis is not constructing a simulation model, but to state the use of simulation and multi-objective optimization in battery designs, this part is not discussed in the main chapters.

3.2 Tuning Parameters

Before constructing an optimization problem, the tuning parameters needs to be discussed and addressed.

In different literatures, the values of solid phase diffusion coefficients (D_{sp}, D_{sn}) often vary from one to another [25][26][27][28]. To assess the influence of D_{sp} and D_{sn} to discharging curves in our simulation model, a simple experiment was performed. Figure 3-2 shows the influence of D_{sp} to the discharge curve at a discharge rate of 1C. In this figure, the value of D_{sp} varies from 1×10^{-18} to 7×10^{-18} m^2/s. Obviously, the change of D_{sp} only has a little influence on the beginning part the discharge curves, while the remaining parts of discharge curves are almost the same for different D_{sp} values.

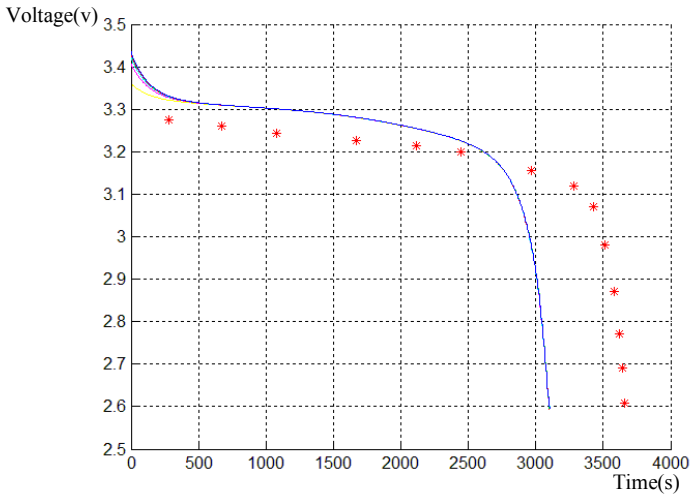

Figure 3-2 Influence of Dsp to 1C Discharge

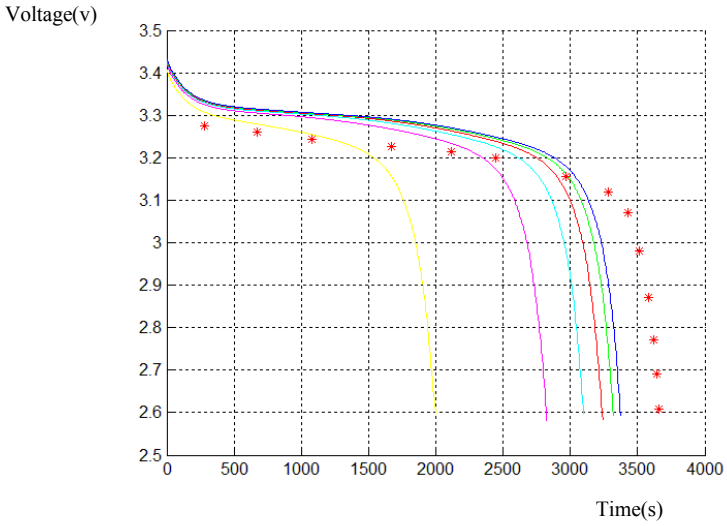

Figure 3-3 Influence of Dsn to 1C Discharge

On the other hand, Figure 3-3 shows the influence of D_{sn} to the discharge curve at the discharge rate of 1C. In the figure, the value of D_{sn} varies from 1×10^{-14} to 7×10^{-14} m^2/s while the other parameters are kept as constants. As can be observed, the change of D_{sn} has a great impact to the discharge curves in our model.

Thus, although both D_{sn} and D_{sp} vary among literatures, based on the influence in our simulation model, only D_{sn} is selected as one of the tuning parameters.

In our model, the exchange current densities are determined by the charge transfer rate constants, solid phase concentrations and charge transfer coefficients. For sake of simplicity and as performed in several reported battery models, the exchange current densities have been set as constants in discharging and charging operations[27]. By modifying the values of charge transfer rate constants (k_n^0, k_p^0), an appropriate setting of exchange. As can be shown in Figure 3-4 (varying k_n^0 while keeping the other parameters constant), the influence of k_n^0 to the discharge curves is significant. This kind of influence can be observed for k_p^0 with our simulation model as well. Thus, k_n^0 and k_p^0 are both considered as tuning parameters in this project.

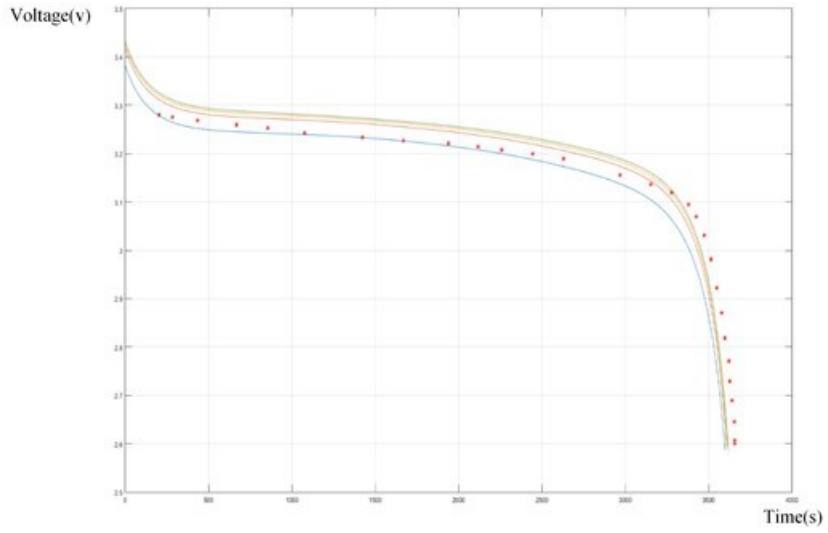

Figure 3-4 Influence of k_n^0 to 1C Discharge

Figure 3-5 shows the influence of the initial value of hysteresis factor ($\Gamma_{discharge}^0$) to the discharge curve at the discharge rate of 1C. Again, only $\Gamma_{discharge}^0$ varies for different discharge curves shown in the figure, the other parameters are kept constant. As can be seen, $\Gamma_{discharge}^0$ has

a significant influence on discharge curves as well. To better reflect the hysteresis phenomena for $LiFePO_4$ batteries, we considered $\Gamma^0_{discharge}$ and Γ^0_{charge} as two different tuning parameters in the model tuning process, the tuning process is expected to give the optimal values for both of these. If the values are close, we can assume $\Gamma^0_{discharge} = \Gamma^0_{charge}$. If not, it will be better to set the initial value of hysteresis factor differently for charging and discharging to get the optimal fit with experimental data.

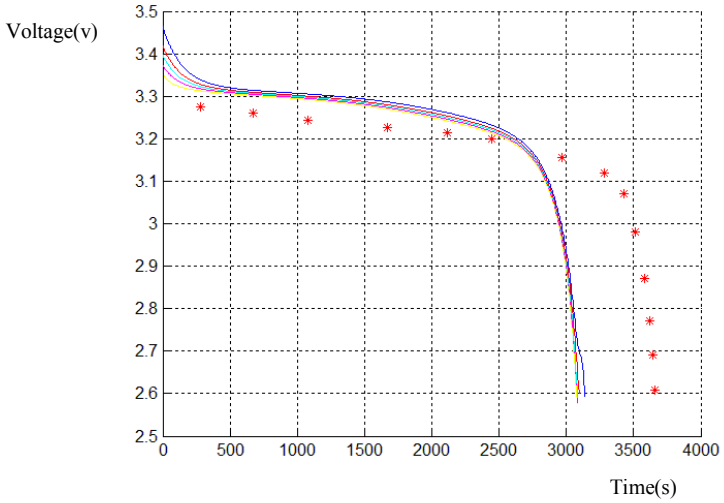

Figure 3-5 Influence of $\Gamma^0_{discharge}$ to 1C Discharge

It is often observed that the experimental discharging curve has a larger drop than the simulation predictions. This offset is explained by contact resistance (R_{con}) in [25]. Thus, R_{con} is considered as another tuning parameter in this project.

As a summary for the above discussion, solid phase diffusion coefficient of negative electrode (D_{sn}), charge transfer rate constants (k_p, k_n), initial values of hysteresis factor for charging and discharging ($\Gamma^0_{charge}, \Gamma^0_{discharge}$) and contact resistance (R_{con}) are considered as tuning parameters in this project.

3.3 Model Tuning and Validation

Forman, Joel C. [24] illustrated a process of using Genetic Algorithm to identify parameter values for $LiFePO_4$ batteries. This thesis also adopts Genetic Algorithm to automate the process of model tuning.

The experimental data used in model tuning is from the figures of Prada's paper [27]. He and his team measured the discharge/charge curves of the commercial LiFePO4-graphite cells ANR26650M1 from A123 systems for the discharge/charge rates of 0.25C, 0.5C, 1C, 2C, 4C and 8C. The curves reported by him are used as the reference for our simulation model, Table 3-1 gives all the data points we picked from his discharge/charge curves for model tuning.

Based on the observation, the predicted discharge curves of our simulation model often become fluctuating rather than a smooth decreasing curve when the discharge rate is as high as 8C. Also, the charging curve for the rate of 8C is very steep and ended prematurely [27]. The tuning is thus limited to the discharge/charge rates up to 4C.

For each discharge/charge rates, the sum of squared residuals between model predictions and experimental data can be calculated by

$$SSE_{rate} = \sum\left(PV_{t_i}^{d} - EV_{t_i}^{d}\right)^2 + \sum\left(PV_{t_j}^{c} - EV_{t_j}^{c}\right)^2 \qquad (3\text{-}1)$$

Where $PV_{t_i}^{d}$ and $EV_{t_i}^{d}$ are predicted and experimental voltages on the discharge curve at time t_i, $PV_{t_j}^{c}$ and $EV_{t_j}^{c}$ are predicted and experimental voltages on the charge curve at time t_j. Since the predicted voltage values vary when the tuning variables are changed, SSE_{rate} can be expressed as a function of tuning variables we discussed in Section 3.2.

$$SSE_{rate} = f_{rate}(D_{sn}, k_p, k_n, \Gamma^0_{charge}, \Gamma^0_{discharge}, R_{con}) \qquad (3\text{-}2)$$

Where the function of f_{rate} is based on the responses of our simulation model. Thus, the objective function used for model tuning is set as

$$Minimize\ SSE_{total} = SSE_{0.25C} + SSE_{0.5C} + SSE_{1C} + SSE_{2C} + SSE_{4C} \qquad (3\text{-}3)$$

The function of ga in MATLAB is used to implement the genetic algorithm for model tuning. As boundary constraints (see Table 3-2) exist, the adaptive feasible mutation function implemented in MATLAB is used for mutation. To expand the range of searching, the population size is set as 200. To make sure the algorithm is terminated within an acceptable time scale, the maximum generation is set at 50, the terminated tolerance for objective function is set as 1e-3, the stall generation limit is set as 20. We want to explore more feasible values, so the fraction of mutations in the sons is increased to 20%. To make sure the elite individuals can survive through generations, the elite count is chosen as 5. Intermediate function is chosen as the crossover function. To speed up the algorithm, parallel computing is used so that multiple individuals can be measured at the same time. Table 3-2 summarized the results from the genetic algorithm, these parameter values give relatively good fitting for simulation predictions to the experimental data, the optimized SSE_{total} is 0.7190.

Table 3-1 Experimental Data for Model Tuning

0.25C				0.5C				1C			
Charge		Discharge		Charge		Discharge		Charge		Discharge	
time	voltage	time	voltage	time	voltage	time	voltage	time	voltage	time	voltage
111.381	2.819	528.079	3.334	19.810	2.777	450.142	3.304	0.960	2.736	202.680	3.279
182.918	2.905	758.781	3.325	169.062	3.050	556.662	3.299	9.881	2.796	282.603	3.276
242.561	2.971	1025.120	3.320	228.911	3.102	858.717	3.301	39.699	2.930	433.565	3.269
386.192	3.034	1611.253	3.315	366.693	3.171	1267.239	3.294	60.598	3.004	668.904	3.260
553.812	3.098	2765.911	3.309	726.345	3.263	1595.838	3.288	165.330	3.188	855.399	3.253
685.544	3.143	3494.280	3.308	942.256	3.272	2030.931	3.276	195.282	3.217	1077.400	3.242
1680.676	3.253	4186.750	3.294	1236.111	3.294	2474.934	3.265	246.223	3.252	1423.779	3.234
2040.511	3.263	4914.910	3.285	1685.903	3.322	2901.327	3.265	345.150	3.285	1668.014	3.226
2712.177	3.288	5518.810	3.279	2021.764	3.336	3318.758	3.260	408.120	3.293	1938.912	3.221
3251.930	3.305	6229.308	3.274	2645.544	3.348	3727.307	3.255	504.076	3.305	2116.524	3.214
4295.502	3.326	7117.574	3.272	3353.320	3.351	4073.699	3.251	683.990	3.329	2258.602	3.207
5015.247	3.333	7828.125	3.269	3929.132	3.356	4322.323	3.244	878.903	3.351	2445.097	3.200
5806.997	3.335	8432.077	3.265	4301.003	3.363	4571.000	3.241	1277.756	3.371	2631.566	3.189
6610.740	3.338	9071.562	3.262	4738.847	3.371	4881.781	3.232	1676.625	3.378	2968.878	3.156
7570.444	3.338	9764.137	3.251	5014.735	3.382	5290.225	3.219	1985.520	3.387	3155.282	3.136
8194.241	3.341	10403.413	3.241	5458.580	3.390	6630.515	3.147	2429.365	3.403	3513.901	2.981
8866.009	3.346	11042.584	3.226	6010.392	3.398	7054.765	3.002	2867.207	3.422	3627.514	2.729
9537.778	3.352	11699.522	3.212	6310.280	3.406	7305.786	2.600	3095.119	3.437	3658.363	2.600
9957.608	3.360	12267.680	3.200	6520.188	3.417			3212.061	3.454		
10305.456	3.369	12782.382	3.182	6724.059	3.443			3293.009	3.476		
10905.247	3.374	13386.021	3.168	6873.895	3.489			3346.954	3.505		
11589.025	3.377	13758.122	3.135	6933.742	3.542			3391.887	3.547		
12428.748	3.381	13951.984	3.082	6963.659	3.570			3421.835	3.580		
12932.562	3.387	14180.753	3.008								
13232.453	3.391	14391.180	2.914								
13796.059	3.434	14548.412	2.824								
14011.757	3.480	14634.840	2.743								
14155.374	3.546	14721.216	2.660								
		14740.634	2.600								

2C				4C				8C			
Charge		Discharge		Charge		Discharge		Charge		Discharge	
time	voltage	time	voltage	time	voltage	time	voltage	time	voltage	time	voltage
47.925	3.138	45.729	3.255	1.285	2.899	17.241	3.216	0.903	3.078	6.297	3.105
69.480	3.204	63.449	3.242	4.357	2.942	35.993	3.149	1.667	3.123	21.187	2.997
83.345	3.234	110.034	3.228	7.425	2.994	61.503	3.133	3.202	3.169	36.143	2.960
106.456	3.279	147.761	3.221	12.022	3.093	118.097	3.114	5.315	3.222	47.233	2.944
128.030	3.315	198.827	3.218	18.173	3.153	143.637	3.114	7.621	3.273	62.772	2.937
152.703	3.329	280.990	3.216	28.174	3.235	176.945	3.112	10.119	3.325	82.752	2.930
172.752	3.337	436.406	3.205	38.180	3.300	216.907	3.105	13.388	3.384	98.296	2.928
226.736	3.351	598.485	3.195	47.421	3.347	282.407	3.098	20.318	3.461	117.725	2.925
322.365	3.377	764.993	3.181	59.749	3.389	342.355	3.091	24.744	3.514	142.707	2.923
444.218	3.402	884.883	3.172	75.938	3.415	397.856	3.080	32.643	3.559	174.344	2.912
601.562	3.414	1024.747	3.159	95.989	3.427	470.012	3.069	39.388	3.583	211.528	2.896
775.875	3.425	1106.891	3.152	131.463	3.447	517.740	3.059			252.593	2.875
927.049	3.434	1211.229	3.142	191.619	3.471	556.584	3.048			299.754	2.842
1115.246	3.445	1324.437	3.128	251.778	3.485	619.844	3.031			325.278	2.826
1304.982	3.461	1479.802	3.103	328.907	3.500	679.773	3.013			345.806	2.810
1490.086	3.485	1564.100	3.078	402.180	3.507	716.390	2.999			359.678	2.801
1584.168	3.516	1621.769	3.059	485.480	3.518	752.997	2.979			407.921	2.738
1656.632	3.579	1670.529	3.032	582.663	3.531	799.568	2.944			426.755	2.692
		1694.873	3.009	661.334	3.547	830.588	2.905			435.595	2.644
		1719.177	2.976	721.492	3.564	864.879	2.835				
		1736.820	2.942	766.223	3.583	891.310	2.716				
		1754.436	2.902								
		1772.000	2.847								
		1787.317	2.785								
		1804.789	2.706								
		1816.204	2.600								

Table 3-2 Tuned Parameters for Simulation Model

Parameters	Tuned Value	Lower Bound	Upper Bound
D_{sn}	8.7559e-14	6e-14	9e-14
k_p^0	2.6061e-12	1e-12	1e-10
k_n^0	9.0912e-12	1e-13	1e-10
Γ_{charge}^0	0.1687	0	0.6
$\Gamma_{discharge}^0$	0.5852	0.4	1
R_{con}	0.001	0	0.002

Figure 3-6 to Figure 3-10 shows the comparison between model predictions and experimental data. As can be seen, the model with the tuned parameters gives satisfying fit to charge and discharge curves for the rates up to 4C. The predicted energy produced during discharge is 0.34% less than the experimental data for the discharge rate of 0.25C and 1.62% less for 4C.

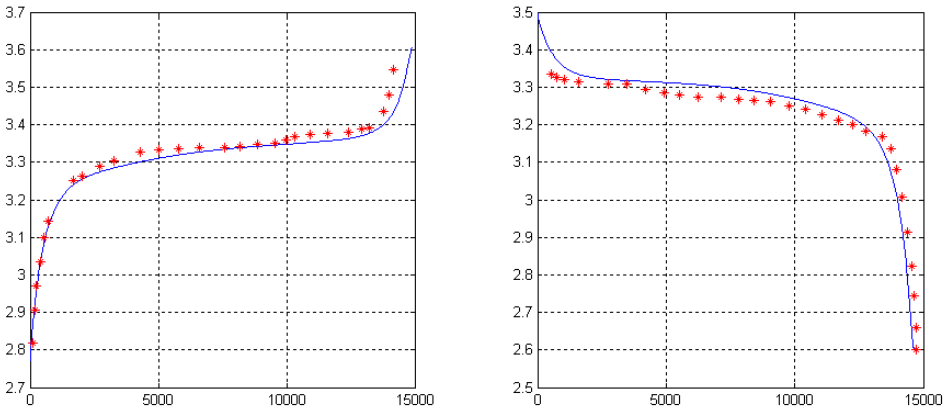

Figure 3-6 Model Fitting at 0.25C

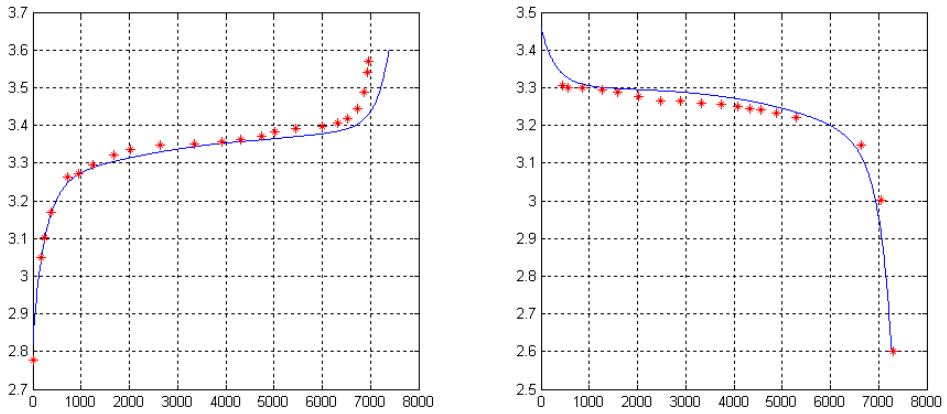

Figure 3-7 Model Fitting at 0.5C

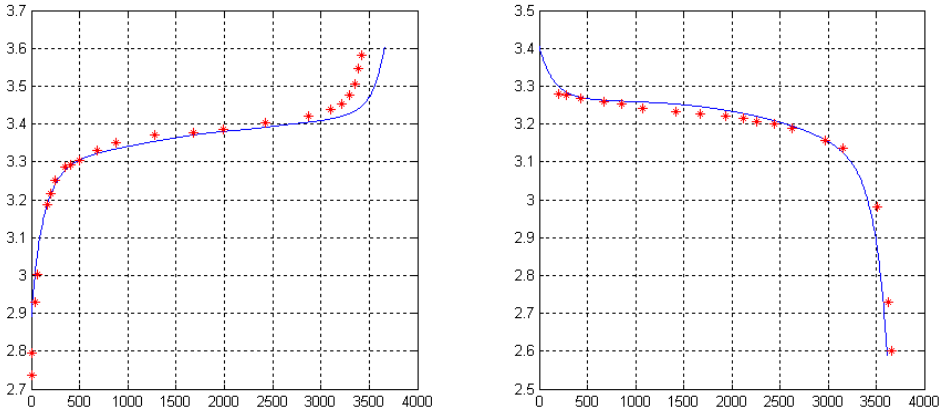

Figure 3-8 Model Fitting at 1C

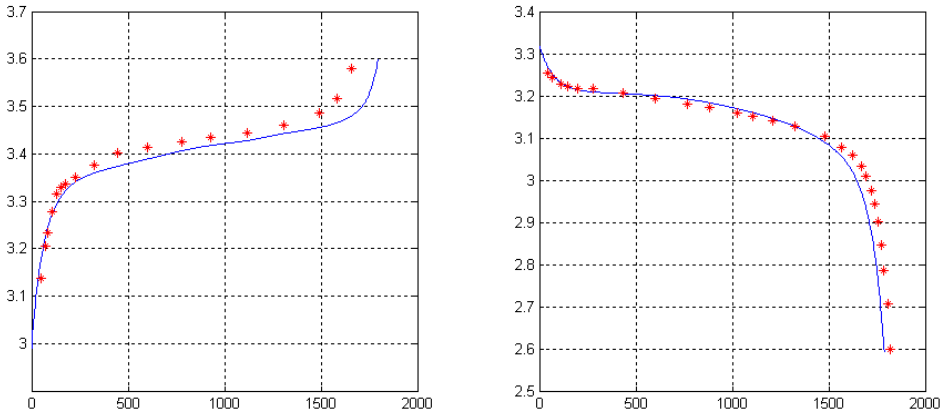

Figure 3-9 Model Fitting at 2C

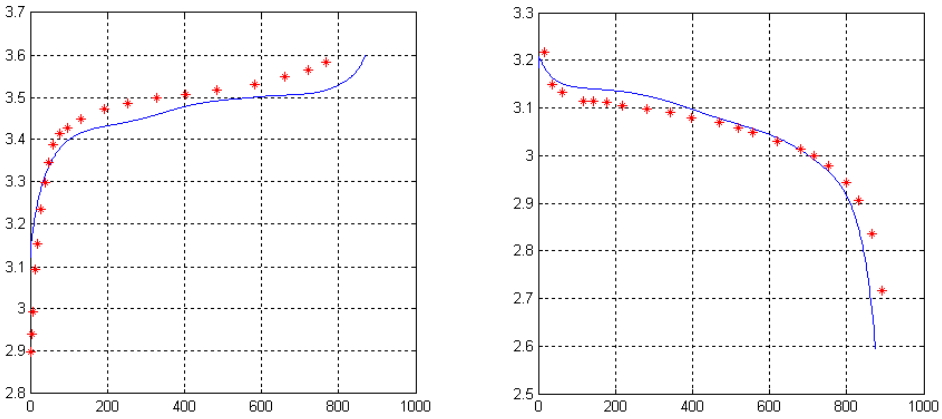

Figure 3-10 Model Fitting at 4C

Figure 3-11 shows the change of the distribution of the optimal 20% individuals from generation to generation. As shown in the plot, at the first several generations, the fitness values for the 20% optimal individuals are scattered. But after a couple of generations, this distribution became more convergent. After 24 generations, the algorithm was terminated because of the minimum tolerance set for the fitness function value was reached. The 20% optimal individuals have been pretty much converged to the optimal solution obtained from the algorithm because of the crossover function.

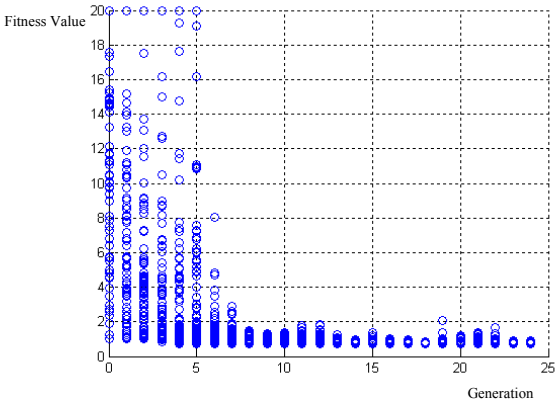

Figure 3-11 Fitness Values for the 20% Optimal Individuals for Each Generation

3.4 Discussion

The process of selecting tuning parameters in this thesis is stated in Section 3.2. When looking for these tuning parameters, our objective is to find the values that give the best fitting for a given design. Thus, parameters that can be considered as design variables, such as thickness of electrodes and particle size, shouldn't be selected as tuning parameters as this can limit the capability of the simulation model when applied for design optimizations. Also, the value of tuning parameters needs to have a great influence on the response of the model so that by changing these parameters, a better fitting between model predictions and experiment data can be achieved. The tuning parameters in this thesis are mostly those that are reported with different values among literatures but have an obvious impact to the predictions of the adopted simulation model. Some of them are measurable according to the literatures, but because of the limits of our project, tuning them to proper values can be the most appropriate way to get a simulation model with a decent precision.

Section 3.3 shows the formula of the optimization problem used for model tuning and the results of the tuning process. Again, a genetic algorithm was implemented with MATLAB to identify the optimal values for tuning parameters. To validate the results, we compared the discharging/charging curves predicted by the simulation with the experimental data from Parada's team [27]. Since more focus will be given to the performance of discharging in this thesis, the errors for energy predictions for different discharge rates are also measured.

Based on the results, the tuned simulation model gives both great fitting for discharge/charge curves and minor errors in energy predictions for the rates up to 4C. To make sure the solution of genetic algorithm was convergent, the fitness values of the 20% optimal individuals for each generation were recorded and plotted in Figure 3-11. As can be shown,

because the population size was chosen properly, the algorithm converged to the optimal solution within an acceptable number of generations.

After the tuning process, it is convincing to state that the simulation model is well capable in predicting the performance for the modeled $LiFePO_4$-graphite system for discharging rates up to 4C. The tuned simulation model is going to be adopted for quantitative discussion of multi-objective optimal design for lithium-ion battery cells in the thesis. Chapter 4 will illustrate the application of this model and the optimal designs obtained.

Chapter 4. A Three-Objective Optimization Problem and Its Quantitative Analysis for $LiFePO_4$-Graphite Cell Optimal Designs

In Chapter 3, an DAE-based simulation model was introduced. After model tuning, it has shown a good capability in predicting the discharge curves for the cycling rates up to 4C. This tuned simulation model is employed for the quantitative analysis based on multi-objective optimization problems for the $LiFePO_4$-graphite battery optimal designs.

The two-objective optimization problem constructed in Chapter 2 is modified to fit the current simulation model structure and solved with the assistance of the high precision simulation model and genetic algorithm in Section 4.1. The shape of the Pareto front validates the qualitative analysis in Chapter 2.

Then a three-objective optimization problem is constructed in Section 4.2 and solved in Section 4.3. This problem measures the cell performance for both high and low current discharge in terms of with energy per unit separator area. To control the weight of the cell design, minimizing the mass per unit separator area is still considered as another objective. The resulted Pareto front comes out to be a surface in the 3D space. Then, the application of the obtained Pareto front is discussed in Section 4.4. At last, more discussions regarding the procedures and solutions are given in Section 4.5.

4.1 Validating the Pareto Front for the Two-Objective Design problem

In Chapter 2, we constructed a two-objective optimization problem for lithium-ion battery cell optimal design with the objectives of maximizing the specific energy per unit separator area for the discharge rate of 0.5C and minimizing the mass per unit separator area. With the assistance of a simple reaction zone model and genetic algorithm, we were able to qualitatively analyze the shape of the Pareto front for this optimization problem. Based on the solutions, the Pareto front was identified as a concave curve in a 2D plane.

Now that a precise simulation model was constructed and tuned in Chapter 3, we are allowed to quantitatively solve the two-objective optimization problem constructed in Chapter 2 and validate the results and analysis that were illustrated and discussed before. Also, since the model is now able to handle more design variables besides porosity and thickness of positive electrode, we can further validate the discussions in Section 2.5.

The design variables considered include particle radius of positive and negative electrodes (R_p, R_n), porosity of both electrodes (ϵ_p, ϵ_n) and the thickness of positive electrode (L_p) are considered.

To simplify the problem, the volume fraction of fillers (ϵ_{effp}, ϵ_{effn}) are fixed as constants. The thickness of negative electrode (L_n) is changed to maintain the balance of cyclable Li between the two electrodes (see Equation 57 and Equation 58 in [27]).

Thus, the two-objective optimization problem constructed in Chapter 2 now can be represented with the following formulas:

$$maximize\ E_{0.25C} = g_{0.25C}(R_p, R_n, \epsilon_p, \epsilon_n, L_p) \tag{4-1}$$

$$minimize\ M = h(\epsilon_p, \epsilon_n, L_p) \tag{4-2}$$

Since the purpose of this section is to validate the former results, the definition of function g_{rate} and h, or how to measure the specific energy and mass per unit separator area for a given design are illustrated in Section 4.2, where a new three-objective optimization problem is constructed and introduced. To be concise, these contents are omitted in this section.

Figure 4-1 shows the resulted Pareto front of the "base problem" in Chapter 2 with the tuned DAE based simulation model and the genetic algorithm. As can be observed, the shape of Pareto front is similar with the qualitative results obtained before. This validated the results and discussions in Chapter 2. Based on the case study in Section 2.4, we should be able to apply this quantitative results to multiple design cases regarding different target applications.

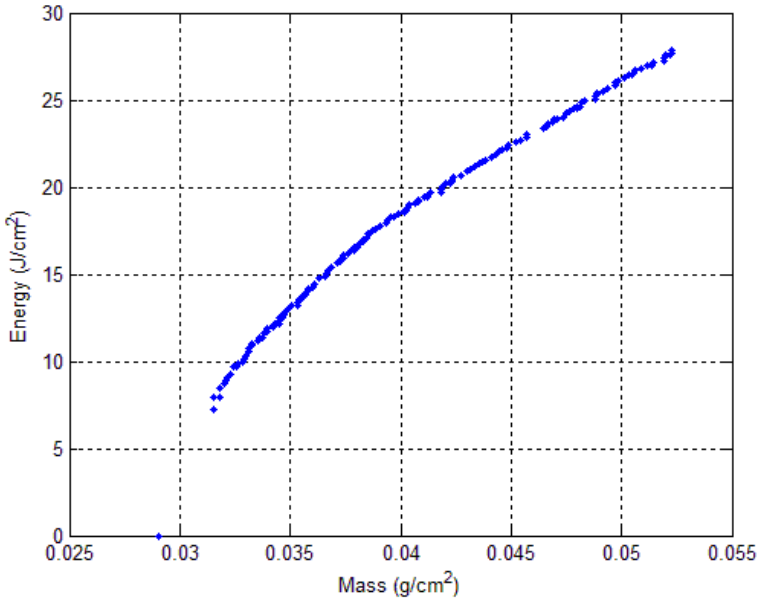

Figure 4-1 Validating the Results of the Two-Objective Optimization Problem in CH 2

4.2 Construction of a Three-Objective Design Problem for LiFePO4-Graphite Li-Ion Batteries

The two-objective optimization problem solved in Section 4.1 measured only the energy performance of low rate energy performance. However, lots of researchers have been interested in high power performance of lithium-ion batteries as well [7, 10, 13]. A good measurement for high power performance of a lithium-ion battery is the peak specific power. It was measured in [7] by discharging the cell until it reaches 80% DOD with a rate of $\frac{1}{3}$C and then finding the current under which the cell reaches the cutoff potential in exactly 30 seconds (or a short time duration). The process of finding the proper current, however, is a trial-and-error procedure and is very computationally expensive and tedious. In [13], the authors proposed a simpler process of using a high-rate pulse (10C for example) to estimate the high power performance of the batteries.

Under an optimization context, it will be too difficult to find the exact pulse current for each design. Thus, the energy per unit separator area for 0.25C discharge is considered as a measure of the slow discharge performance of the battery, and energy per unit separator area is considered as a measure of fast discharge performance of the battery. Obviously, both of these energy measures are expected to be maximized by optimizing the design variables. Although it was stated in [13] that the pulse current should be at least 5C to best estimate the resistance at high rates, 4C is used in this research because the model was tuned only for the rates up to 4C and moving to larger discharge rates may result in validation issues for the simulation model itself. Minimizing the mass per unit separator area is again considered as an objective so that the weight of obtained designs will not be prohibitively heavy.

The design variables referred in Section 4.1 are again considered in the three-objective optimization problem, which are particle radius of positive and negative electrodes (R_p, R_n), porosity of both electrodes (ϵ_p, ϵ_n) and the thickness of positive electrode (L_p) are considered. To simplify the problem, the same assumptions for determining the thickness of electrode (L_n) for a given design employed in Section 4.1 is employed in the three-objective problem construction.

A three-objective optimization problem can be thus constructed based on the former illustration.

$$maximize\ E_{0.25C} = g_{0.25C}(R_p, R_n, \epsilon_p, \epsilon_n, L_p) \tag{4-3}$$

$$maximize\ E_{4C} = g_{4C}(R_p, R_n, \epsilon_p, \epsilon_n, L_p) \tag{4-4}$$

$$minimize\ M = h(\epsilon_p, \epsilon_n, L_p) \tag{4-5}$$

Equation (4-3) and Equation (4-4) are the two energy performance measures and both of them are expected to be maximized. Specifically, the calculation of energy is given in Equation (4-6).

$$E_r = \frac{\sum\left[(I1C\times r)\times\frac{(V_j+V_{j+1})}{2}\times dt\right]}{A} \tag{4-6}$$

$I1C\times r$ is the discharge current. $I1C$ is the discharge rate for 1C, it is assumed to be proportional to the volume of active materials. r is the discharge rate, for simplification, we assumed the discharge current is proportional to discharge rate. dt is the time interval between two voltage predictions, we used 5 sec for 1C discharge, for the other discharge rates, $dt = 5\times rate$ sec. $\frac{V_j+V_{j+1}}{2}$ is the average voltage for the jth time interval. A is the separator area, which is a constant in this paper. The basic concept of this calculation is to divide the whole discharge curve into tiny pieces. By using the average voltage for each tiny piece, the energy in every time

interval can be estimated, and the sum of these estimated energy values will be an estimated energy for the full discharging process. Since dt is small, the estimated energy will be very close to the real value.

The mass calculation is considered to be the sum of the mass of four parts in a battery cell: positive electrode, negative electrode, separator and remaining materials (current collectors, coat etc.).

$$M = M_p + M_n + M_s + M_r \tag{4-7}$$

For positive and negative electrodes, three parts are considered in mass calculation: filler, electrolyte and active materials.

$$M_p = \left(\rho_f \epsilon_{fp} + \rho_e \epsilon_{ep} + \rho_{ap} \epsilon_{ap}\right) L_p A \tag{4-8}$$

$$M_n = \left(\rho_f \epsilon_{fn} + \rho_e \epsilon_{en} + \rho_{an} \epsilon_{an}\right) L_n A \tag{4-9}$$

Where ρ_f, ρ_e and ρ_{ax} $(x = n, p)$ are the density for filler, electrolyte and active materials, the density values used in mass calculation are summarized in Table 4-1. $\epsilon_{fx}, \epsilon_{ex}$ and ϵ_{ax} are the volume fractions for filler, electrolyte and active materials. For each electrolyte, these three should add up to 1. L_x is the thickness for electrode x and A is the separator area and it is a constant ($0.18\ m^2$) in this paper.

Table 4-1 Density Values Used in Mass Calculation

ρ_f	Density of filler(SiO2)	2.65 g/cm^3	Wiki
ρ_e	Density of electrolyte	1.071 g/cm^3	Calculated by 1:1 (w:w) of EMC and DMC
ρ_{ap}	Density of LiFePO4	3.60 g/cm^3	[7]
ρ_{an}	Density of graphite	2.27 g/cm^3	[7]
ρ_s	Density of separator	0.9 g/cm^3	[7]

It is assumed that no filler is contained in the separator, so the mass the separator is the sum of the porous separator materials and the electrolyte. Because no variables used is changed for different designs, the mass of the separator is thus a constant in this paper.

$$M_s = (\rho_s \epsilon_s + \rho_e \epsilon_{es}) L_s A \tag{4-10}$$

The mass of the remaining materials is assumed to be unchanged for different designs and the value ($M_r = 24.219g$) is calculated by the default design [27].

A three-objective optimization problem is thus constructed with all the aforementioned performance measures and assumptions. In the Result section, this optimization problem will be quantitatively solved with the assistance of tuned DAE based simulation model and GA and the property of the Pareto front will be discussed.

4.3 Pareto Front of the Three-Objective Design Problem

In Section 4.1, we quantitatively solved the two-objective optimization problem for optimal lithium-ion battery design constructed in Chapter 2 with the tuned simulation model for a LiFePO4-graphite cell. It was shown that the Pareto front is a concave curve in a 2D plane, which validate the qualitative results in the former chapter [29]. The purpose of this section is to solve the three-objective optimization problem in Section 4.2. Since one more objective is considered in this problem, to visualize the Pareto front, a 3D plot is needed. According to the discussion in Section 2.5, the Pareto front of this problem is expected to be a surface in a 3D space.

The simulation model tuned in Chapter 3 is also used as the tool of quantitative analysis in this problem. With the function of gamultiobj in MATLAB, the genetic algorithm for the three-objective optimization problem is implemented.

It is relatively more difficult to get a smooth three-dimensional Pareto front because the same amount of points appears to be more scarce and divergent in the space compared with a plane, but the computation cost of the employed simulation model, although is massively reduced compared with a P2D model, is still too high for a genetic algorithm with a large scale of thousands of individuals and hundreds of generations.

The population size is set at 350 and the Pareto fraction is set at 0.4 so that more points can be included in the resulted Pareto optimal set, which helps obtaining a relatively smooth Pareto front visually. To make sure the algorithm is terminated in a proper time frame, the maximum number of generations is set at 40. The intermediate crossover function and adaptive feasible mutation are used for generating son generations and the fraction of crossover is 0.8. Boundary constraints are used to decrease the range of searching for the algorithm and summarized in Table 4-2.

Table 4-2 Boundary Constraints for the Design Variables in Optimization

	Lower Bound	Upper Bound	Unit
R_p	1.00E-08	9.00E-08	m
R_n	1.00E-06	9.00E-06	m
ϵ_p	0.2	0.65	-
ϵ_n	0.2	0.6	-
L_p	6.00E-05	1.40E-04	m

Another linear constraint is used because the simulation model works unstably when the volume of active materials is too few, the constraint is given in formula 4-11, where L_p is the thickness of positive electrode, ϵ_p and ϵ_{effp} are the volume fraction of electrolyte and fillers in the positive electrode. Thus $\left(1-\epsilon_p-\epsilon_{effp}\right)$ stands for the volume fraction of the active

materials in the positive electrode and the left hand of the formula gives the volume of active materials included in the positive electrode for each unit separator area. The value on the right side is obtained from an experiment for our simulation model. Most of designs satisfying this constraint can be successfully simulated with the employed simulation model.

$$L_p \times \left(1 - \epsilon_p - \epsilon_{effp}\right) \geq 2.6531 \times 10^{-5} \qquad (4\text{-}11)$$

Figure 4-2 shows the feasible region and the resulted Pareto front together. The feasible region is represented by the red dots, which are a large set of randomly generated designs that satisfied the constraints of the design optimization. The Pareto front is represented by the blue dots, which are the designs included in the Pareto optimal set from the genetic algorithm. As can be seen, the Pareto front is an outer surface of the feasible region where the combinations of the three performance measures are all non-dominated.

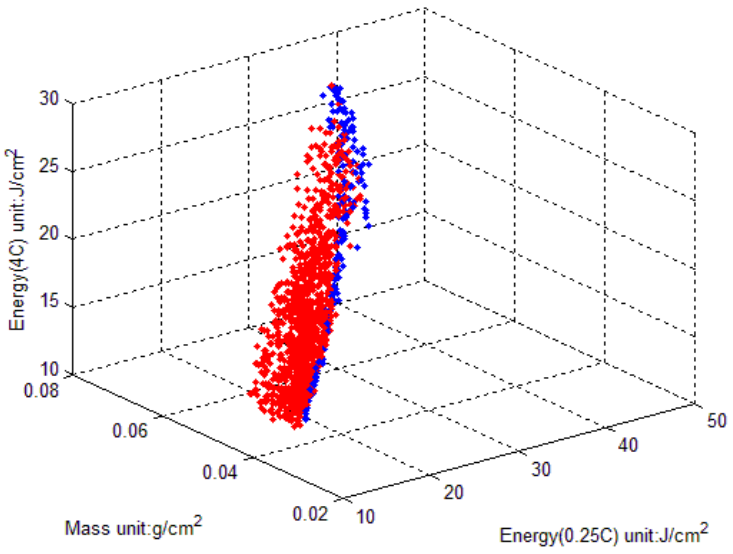

Figure 4-2 The Feasible Region and the Pareto Front of the Design Optimization

In Figure 4-3, the three performance measures are linearly mapped into the interval of [0,1] respectively so that the magnitude difference between the mass and energy measures is compensated. To get rid of the magnitude between the three performance measures helps obtaining a more accurate fitted surface between them. This figure shows how does the Pareto front look like from multiple directions together with the fitted surface for the normalized performance measures. Equation 4-12 gives the polynomial expression of the fitted surface, where x is the normalized 0.25C specific energy per unit separator area, y is the normalized mass per unit separator area, z is the normalized 4C specific energy per unit separator area. The R-square of the fitting is 0.937, the adjusted R-square is 0.9344, both show that the expression is a good fitting to the normalized Pareto optimal set. By observing Figure 4-3, one can also see that the fitted surface well reflects the trends and relationships between the three performance measures.

$$z = 0.001311 + 1.805x + 1.223y - 19.77x^2 + 31.12xy - 14.15y^2 \quad (4\text{-}12)\backslash$$

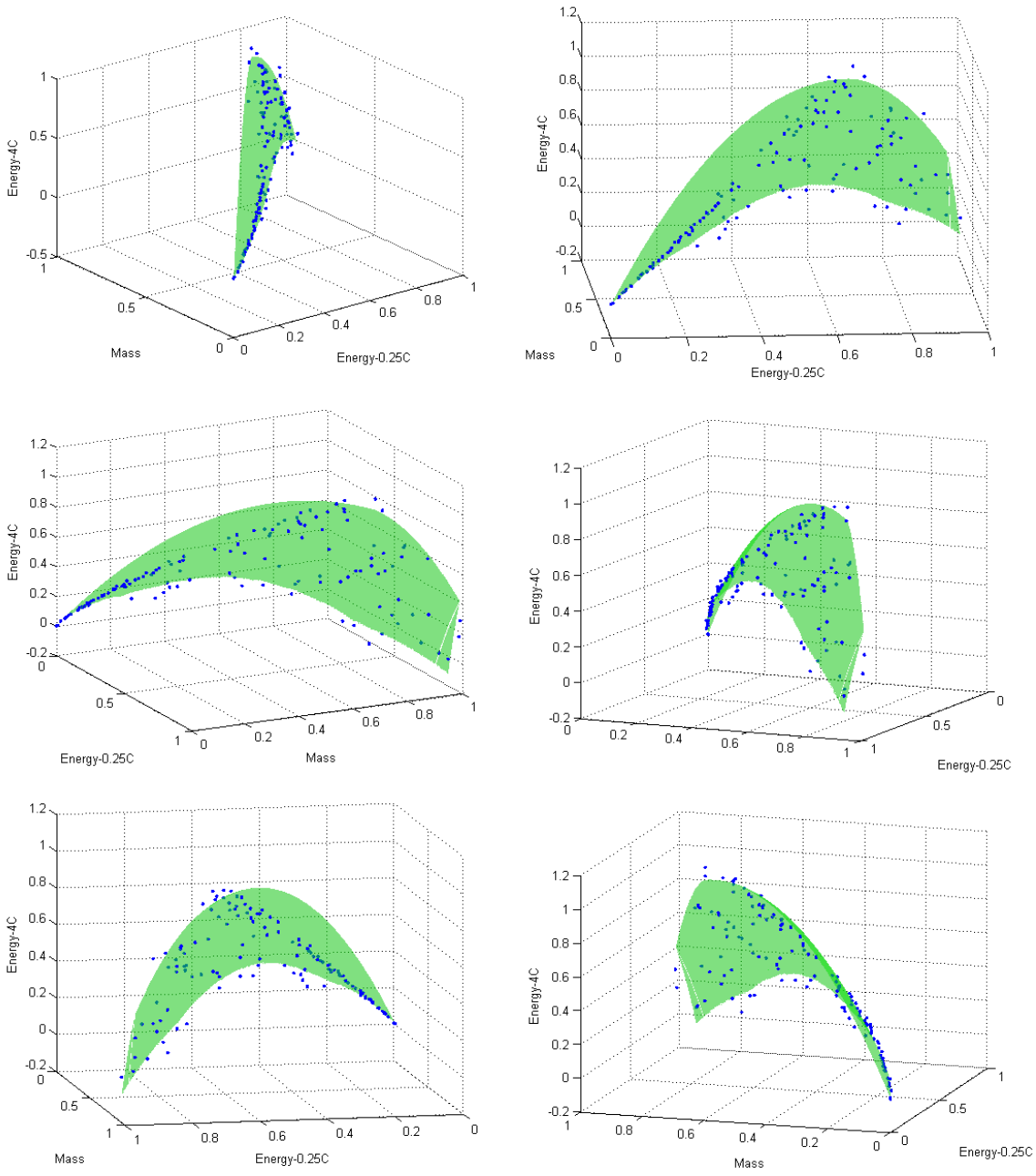

Figure 4-3 Pareto Front of the Three-Objective Problem from Multiple Directions

Figure 4-4 gives the contour plots for the Pareto front obtained from the genetic algorithm and the fitted surface. These contour plots employed the normalized 0.25C and 4C specific energy per unit separator area as *x* axis and y axis and the normalized mass per unit

separator area as the elevation. Plot (a) shows the contour plot of the Pareto front, because of the computation limits, the curves of the contour plot are not as smooth as the fitted surface in plot (b). However, the trends and relationships between the two contour plots are similar to each other, which again validate that the polynomial expression fitted before is a good estimation for the Pareto front obtained by the genetic algorithm. Closely observed, some dominated parts can be identified in both contour plots, this is because to generate these contour plots, MATLAB actually employed some linear interpolation for points located at unknown areas.

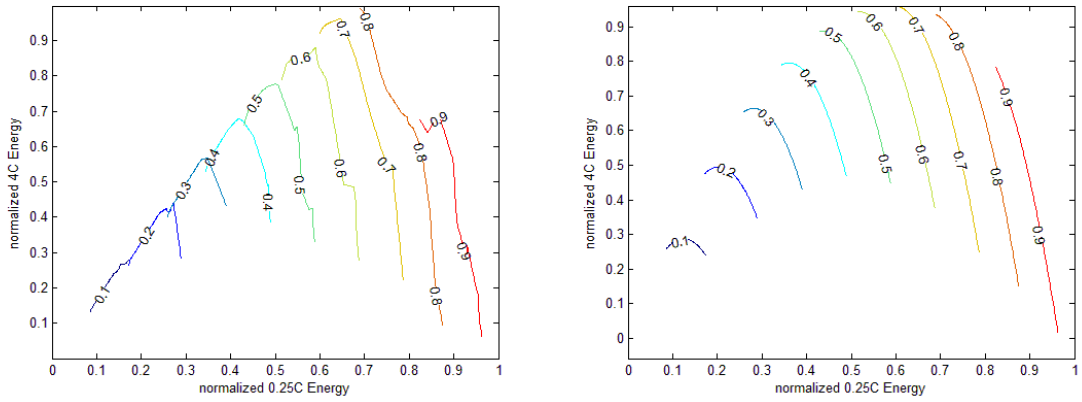

(a) Pareto (b) Fitted Surface

Figure 4-4 Contour Plots of Pareto Fronts and Fitted Surface

As a more complex simulation model is employed here in the optimization process, the computation time is massively increased because the DAE based simulation model is much more inefficient than a reaction zone model or an SP model. Using a desktop with the CPU of Intel Core i7-4790 and a memory of 16.0 GB, the time consumed to estimate the Pareto front was 17.03 hours when a parallel pool of 4 workers was used in the genetic algorithm.

The results of this section validated the former analysis and expectation. In the next section, we will discuss the application of the Pareto front obtained in this section. We will see

that although the computation costs of solving a multi-objective optimization problem is expensive, this disadvantage can be compensated as the solutions to one problem can be applied in multiple design problems in the industry.

4.4 Properties and Applications of the Pareto Front

Based on the results of Section 4.3, the Pareto front of the three-objective optimization problem for the $LiFePO_4$-graphite cell optimal design comes out to be a curved surface in a 3D space. Some discussion about the property and the application of this surface will be discussed in this section.

First of all, the Pareto front given by Figure 4-3 consists of the trade-offs between the three performance measures. The "thin" designs are lighter, but they could not store lots of energy because the lack of active materials. The "thick" designs are heavier, but their energy performance measures for both 0.25C and 4C are massively improved because more active materials are now contained in the electrodes. Also, it is possible for these designs to obtain both good 0.25C and 4C energy performance according to the shape of the Pareto front. The "thicker" designs can store even more energy theoretically. However, it seems that the energy stored in the cell can only be fully utilized with small discharge rate, for high discharge rates such as 4C, their energy performance becomes even worse when the cells are relatively lighter.

Figure 4-5 is the projection of the Pareto front to the plane of mass per unit separator area and 4C energy per unit separator area. This figure clearly shows that the increasing trend of 4C energy performance is stopped and a decreasing trend shows up. An intuitive explanation to this phenomenon is that when the battery cell gets too thick (to contain more active materials within a unit separator area), the influence of the internal resistance of the cell becomes significant for large discharge currents so that the cutoff voltage is reached early in a discharge cycle. This

resulted in the incomplete utilization of active materials in the electrodes. Appendix III discussed this phenomenon mathematically with the simple reaction zone model.

Thus, even though the volume of active materials is further increased, the high rate discharge rate can utilize even less than it used to, which brings the decreasing trend of the projected Pareto front. The same effect, of course, should influence the low rate discharge as well. But to significantly influence the low rate energy performance, the electrodes need to be much thicker, and that part of region shall not be included in the Pareto front because all three objectives are becoming worse when this influence becomes significant for low discharge rates.

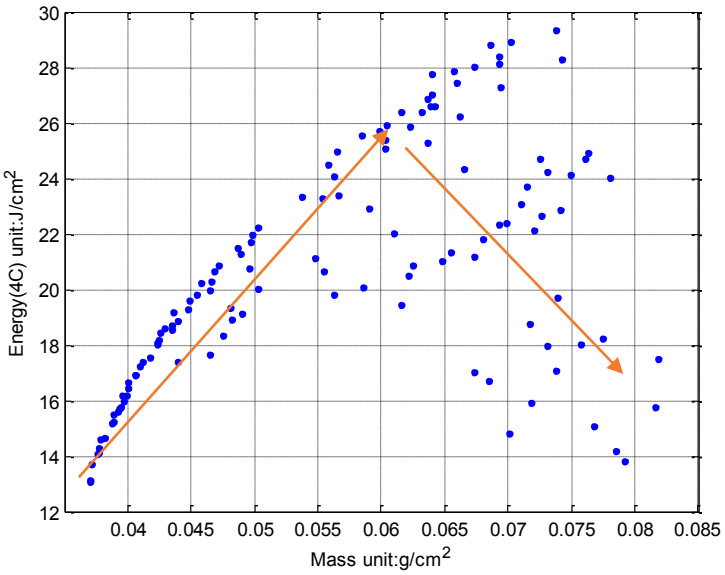

Figure 4-5 The Projection of the Pareto Front to The Plane of Mass Per Unit Separator Area and 4C Energy Per Unit Separator Area

Another valuable discussion may be to explore the correlation between design variables for the solutions in the Pareto front because this kind of correlations may offer some perspectives to designers so that they can better understand the properties of battery cells and guide the proper design of experiments (DOE) for design purposes.

Figure 4-6 plotted the particle radius of negative electrode versus the thickness of negative electrode for the obtained Pareto optimal set. A negative correlation can be observed between these two design variables among the Pareto optimal set which is represented by the trend line in the figure. An explanation to this phenomenon is that the particle radius needs to be reduced when the electrode is thicker to compensate the influence of increased cell internal resistance, especially for high discharge rates such as 4C.

Figure 4-7 shows that the similar correlation exists between the particle radius and the thickness of the positive electrode as well.

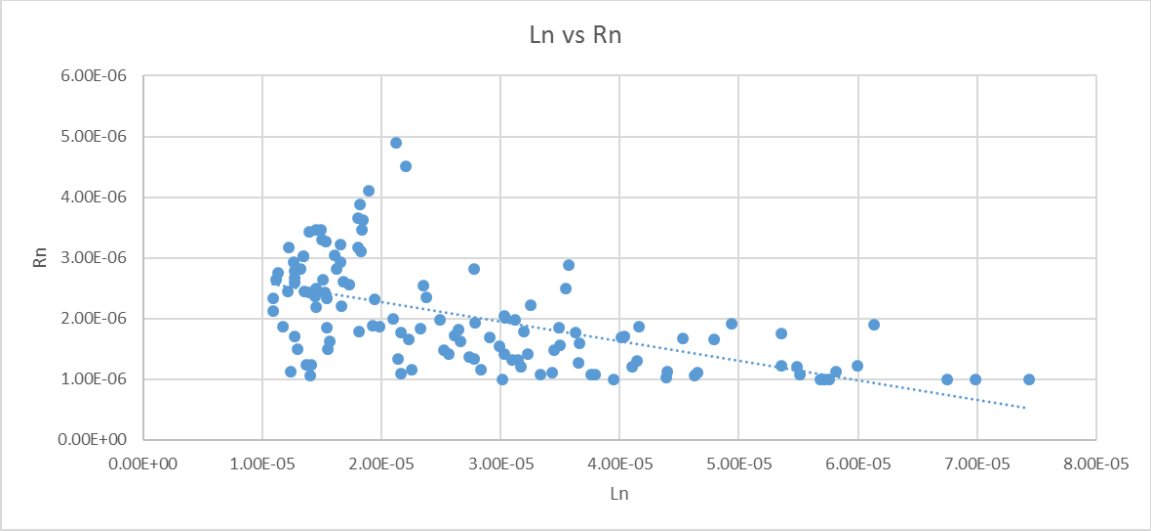

Figure 4-6 Correlation Analysis between the Particle Radius and the Thickness of the Negative Electrode

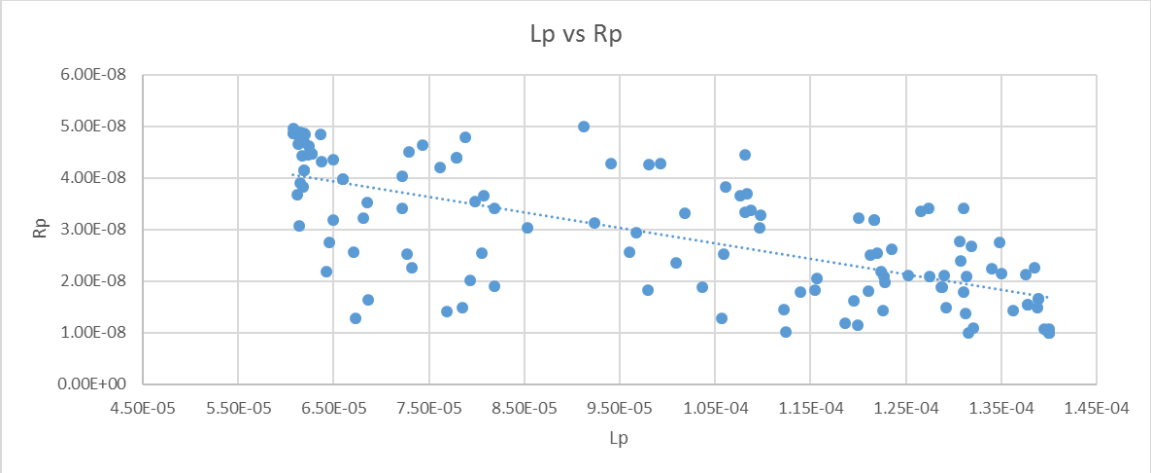

Figure 4-7 Correlation Analysis between the Particle Radius and the Thickness of the Positive Electrode

On the other hand, a positive correlation can be identified between the porosity and the thickness of the negative electrode. When the negative electrode tends to be thicker, it is more likely that a good design needs to have a larger volume fraction of electrolyte in the electrode. This correlation can be identified from Figure 4-8. An explanation to this phenomenon is that more electrolyte is needed to improve the conductivity in the liquid phase of the electrode to compensate the increased liquid phase ohimic resistance of thicker electrode.

One problem is, however, the similar positive correlation was not observed for the porosity and the thickness of the positive electrode. In figure 4-9, we can see that the trend line is almost horizontal, meaning there is no obvious correlation between the two design variables. The possible reason for this is that more fillers are contained in the positive electrode in the simulation model, which may already massively reduce the resistance in the liquid phase of the positive electrode and the necessity to increasing the volume fraction of electrolyte is not as much as that in the negative electrode when the electrodes get thicker.

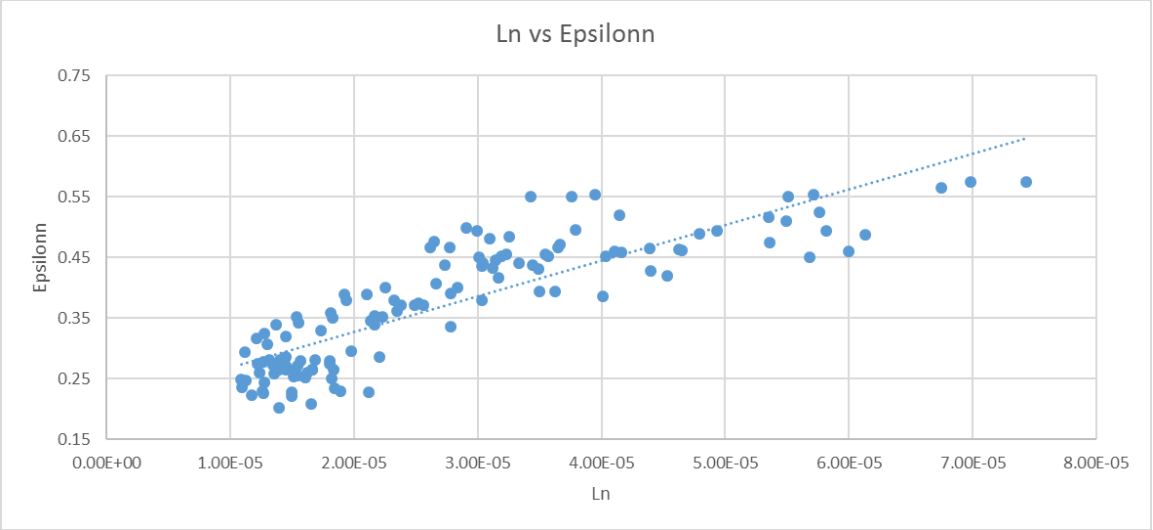

Figure 4-8 Correlation Analysis between the Porosity and the Thickness of the Negative Electrode

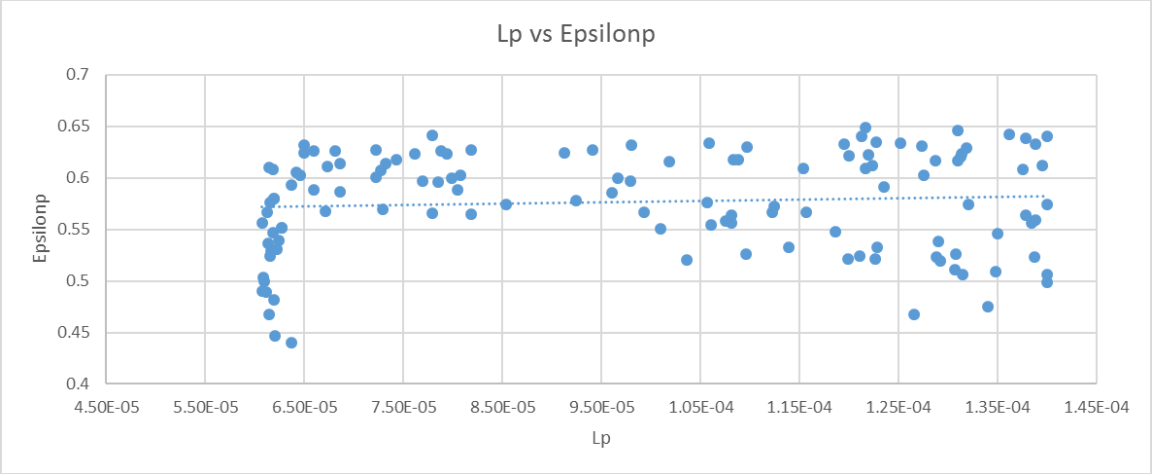

Figure 4-9 Correlation Analysis between the Porosity and the Thickness of the Negative Electrode

It is beneficial to understand that no matter what kind of target application is a certain design used for, it should always be selected from the Pareto optimal set as long as the performance measures that we care about for the target application is the same with the three-objective optimization problem constructed before. Because if it's not in the Pareto optimal set, an alternative design that dominates this one can always be identified by definition, and there is

no reason to select the design that is worse in every aspect that the designers care about. Of course, a different design may be considered when different performance measures are considered. That, however, should be based on a different multi-objective optimization problem.

Even though all the designs should be selected from the Pareto optimal set obtained for different kinds of target applications, the designers may focus on different part of the Pareto front when the target application differs. For example, regarding wearable devices such as smart watches, it might be more important to achieve a light design even when a better energy density can be acquired by adding more active materials into each unit separator area. In this case, the part A in Figure 4-10 may be more promising.

On the other hand, for EV applications, since bigger and heavier designs are allowed to maintain a better specific energy for both high and low discharge rates operations, designers may be more interested in part B because both high and low discharge rates performance are massively improved in this area compared with part A and it is achievable to maintain a good balance between high and low discharge rates performance for these designs when the mass of the battery is controlled as it has to be moved all the time in this application.

Also, in some applications, the weight of the battery cell and the high rate performance may be not important at all, but the size of it needs to be limited (smaller separator area [29]), part C might be better. A solar power traffic light can be a good example, the battery shouldn't be too big, otherwise it will take too much space. But the weight of the cell is not important because there is no need to move it all the time. No high rate operation is needed in this case as well. All these considerations make part C a more promising area for this kind of applications.

In this section, the properties and the applications of the Pareto front for the three-objective optimization problem are discussed, these illustrations are expected to offer some

perspectives and reference for the product design in the industry. The next section will illustrate the advantages and limitations of this study. The possible improvement of future studies will also be discussed in the following section.

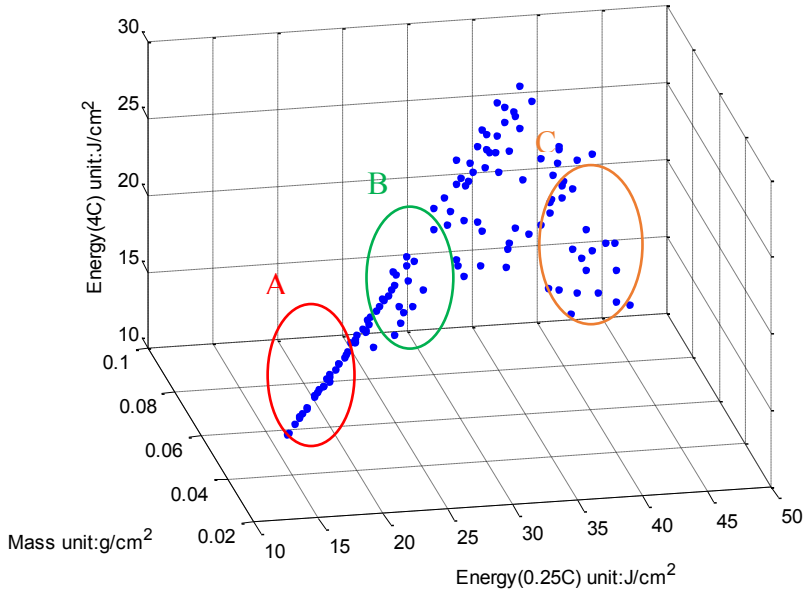

Figure 4-10 The Use of the Pareto Front for Different Target Applications

4.5 Discussion

In this Chapter, we firstly validate the quantitative analysis for the two-objective optimization problem constructed in Chapter 2 with the tuned DAE based simulation model. The Pareto front for the two-objective optimization problem comes out to be a concave curve as expected. Then a three-objective optimization problem was constructed and quantitatively solved in Section 4.2 and 4.3. This problem employed the low discharge rate energy performance, high discharge rate energy performance and the mass performance (all in the unit separator area domain) as its objectives. Comparing to the two-objective optimization problem which considered only the energy performance for low rate discharge, this three-objective problem can

reflect the performance of the cell in more aspects and is expected to be applicable in more design cases whose target operations are different with each other. The resulted Pareto front is a curved surface in a 3D space. Its properties were illustrated in Section 4.4. Also, when the target application is different, it was recommended that the product designers should pay attention to different parts of the Pareto front.

The most significant advantage of applying such a multi-objective optimization process in the lithium-ion battery design, or any other product optimal designs, is that the solutions obtained are not a single point, but a set of trade-offs that are equally good if no preferences are given to multiple contradictory objectives. With the discussion in Section 2.4 and Section 4.4, it is already clear that compared with the single-oriented studies, this kind of process offers more flexibility to the designers as the solutions to a single problem can be applied in many different design cases. Under a product design context, it is hardly that the designers will pay attentions to only one performance measures, there are almost always multiple objectives that have to be considered for a proper product design. These designs are often contradictory in one way or another. An important problem for the real world product optimal design is that it is often difficult for the designers to decide the weight of contradictory performance measures and sometimes even certain objectives are preferred, the other performance measures may have to be at least above some requirements. This problem makes integrating all the objectives into one and transforming a multi-objective optimization problem very difficult. The multi-objective optimization problem, is a good way to start the study of such optimal design problems. By summarizing the properties of Pareto front, the designers are allowed to pick up the most appropriate designs for their target applications or further construct a single-objective oriented

study under the guidance of the Pareto front (proper constraints or objective functions) or design of experiments (DOE) to continuously optimize the designs.

This advantage, however, comes with a much more expensive computation cost. To solve a multi-objective optimization problem is often difficult. As we can see, it is already hard to obtain a smooth Pareto front for a three-objective optimization problem, while in the real industry, tens of performance measures may have to be considered in a single optimal design problem. Although the high computation cost can be partially compensated by the wide applicability of the Pareto front, it is still recommended to pick up the most few important performance measures to construct a multi-objective problem for the optimization and try to control the others with constraints during the algorithm.

Another disadvantage of this process is that no algorithms can so far precisely obtain the Pareto front. The output of genetic algorithm or any other heuristic algorithms is just an estimation of the Pareto front. This problem is true for single-objective oriented studies as well. But when more objectives are considered, it is more difficult to obtain a good estimation to the Pareto front. However, as long as a set of satisfying designs can be identified with the algorithms, it will not be that important to accurately obtain the true Pareto front in the real design context.

This study employed a DAE based simulation model as the tool. As there are some limitations with the simulation model, such as its instability when high cycling rate (8C) is used for charging and discharging and when the active materials contained in the electrodes are too few, the feasible region of the problem may be limited because of the improper objective setup and extra constraints. However, the purpose of the study is to illustrate the process of applying multi-objective optimization to optimal product designs with the assistance of simulation models.

The advantages and disadvantages of the process can still be well discussed with the results of this study.

The future study should be focused on better simulation capability and problem construction. A better simulation model helps reducing the computation costs and improving the ability of exploring the feasible region of performance measures. A more appropriate problem construction makes the solutions applicable for different design problems in the industry, which may compensate the high computation cost of multi-objective optimization better. Also, when the problem is properly constructed, the resulted optimal designs will be more competitive in the market

.

Chapter 5. Summary

This is a summary chapter, where the results and conclusions of former chapters are illustrated in Section 5.1, the defects of the current project and the possible future efforts are discussed in Section 5.2.

5.1 Summary of Results and Conclusions

A two-objective optimization problem was firstly constructed in Chapter 2. The two performance measures considered were maximizing the energy produced per unit separator area in a cycle with the discharge rate of 0.5C and minimizing the mass per unit separator area. To illustrate the properties of the Pareto front and advantages of employing multi-objective optimization in the design process without consuming too much time, the simple reaction zone model was used to simulate the discharge process of the lithium ion batteries. The genetic algorithm in the global optimization toolbox of MATLAB was used to solve the two-objective optimization problem. Because of the simplicity of the reaction zone model, this chapter only delivered a preliminary qualitative analysis, but the results showed that the Pareto front for the two-objective optimization problem looks like a concave curve in the 2D plane of the two performance measures. With three case studies, the obtained Pareto front was applied to three design projects with different target applications. The solutions to a well-constructed multi-objective optimization problem not only gives the researchers the extended flexibility of selecting trade-offs among contradictory performance measures, but also offers the potential of solving multiple different problems simultaneously in the industry. These advantages of

employing multi-objective optimization into product design process were well revealed by the qualitative analysis in the Chapter 2.

However, to find quantitative accurate solutions, the reaction zone model was not adequate. In Chapter 3, a DAE-based PP model for $LiFePO_4$-graphite cell was employed. A process of tuning parameters selection and model tuning was illustrated in this chapter. The criteria used for selecting tuning parameters include: ① the value varies among literatures; ② Change of parameter values influence the discharge curve a lot with the simulation model; ③ parameters were estimated (not exactly measured) in the literature. The model tuning process is basically a optimization process that minimized the sum of squared residuals for the discharge curves and charge curves (time vs voltage) of multiple cycling rates. After the model tuning, the employed DAE based simulation model showed a satisfying precision for cycling rates up to 4C and should be a good tool for quantitative analysis. The tuning process itself, is expected to offer some references to any simulation model tuning problems.

Based on the qualitative analysis in Chapter 2, the advantages of employing multi-objective optimization in the lithium-ion battery optimal design were revealed. With the tuned DAE based simulation model in Chapter 3, a tool for quantitatively accurate analysis was prepared. Thus, the results in Chapter 2 were firstly quantitatively validated in the Chapter 4. Then, another three-objective optimization problem was constructed in Chapter 4. The three objectives considered were maximizing the energy produced per unit separator area in a discharging cycle with both low and high rates (0.25C and 4C) and minimizing the mass per unit separator area. Compared with the two-objective optimization problem, this problem considered not only the energy performance of low discharge rate, but also the energy performance when the cycling rate was high. The Pareto front came out to be a curved surface in the 3D space of the

three performance measures. The properties of the Pareto front were illustrated in the chapter, and a discussion about how to apply this Pareto front on different types of target applications was guided. The wide applicability of the constructed problem was considered to compensate the high computation costs of solving multi-objective optimization problems. The results were expected to offer perspective for LiFePO4-graphite cell designs, the process could offer reference to product designs and design of experiments in the industry.

5.2 Limitations of the Project and Discussion of Future Studies

Although the model tuning process resulted in a simulation model which held a satisfying precision in this study, it is still recommended that more physical or chemical parameters shall be measured if allowed to make sure the simulation model reflects the properties of the materials and chemical reactions more accurately.

Also, there were some instability issues with the DAE based simulation employed, when the active materials in the electrodes were too few, the model may fail to predict a discharge curve, this problem held when the discharge rate exceeded 4C as well.

The way of discussing the correlation between pairs of design variables may be risky as the changes of the other variables were not well controlled when discussing a pair of design variables.

Thus, the future efforts of the study include:

1. Construct better multi-objective optimization problems that can offer a wider applicability in the industry.
2. Employ more stable and quantitatively precise simulation models for problem analysis.

3. Explore better visualization and results analysis methods for optimization problems with multiple dependent and independent variables.

References

[1]. Scrosati, Bruno, and Jürgen Garche. "Lithium Batteries: Status, Prospects and Future." Journal of Power Sources: 2419-430.

[2]. Scrosati, Bruno, Jusef Hassoun, and Yang-Kook Sun. "Lithium-ion Batteries. A Look into the Future." Energy & Environmental Science Energy Environ. Sci.: 3287.

[3]. Christen, Thomas, and Martin W. Carlen. "Theory of Ragone Plots." Journal of Power Sources: 210-16.

[4]. Santhanagopalan, Shriram, Qingzhi Guo, Premanand Ramadass, and Ralph E. White. "Review of Models for Predicting the Cycling Performance of Lithium Ion Batteries." Journal of Power Sources: 620-28.

[5]. Luo, Weilin, Chao Lyu, Lixin Wang, and Liqiang Zhang. "A New Extension of Physics-based Single Particle Model for Higher Charge–discharge Rates." Journal of Power Sources: 295-310.

[6]. Newman, John. "Optimization of Porosity and Thickness of a Battery Electrode by Means of a Reaction-Zone Model." Journal of The Electrochemical Society J. Electrochem. Soc.: 97.

[7]. Srinivasan, Venkat, and John Newman. "Design and Optimization of a Natural Graphite/Iron Phosphate Lithium-Ion Cell." Journal of The Electrochemical Society J. Electrochem. Soc.

[8]. Chen, Y.-H., C.-W. Wang, X. Zhang, and A.m. Sastry. "Porous Cathode Optimization for Lithium Cells: Ionic and Electronic Conductivity, Capacity, and Selection of Materials." Journal of Power Sources: 2851-862.

[9]. Methekar, Ravi N, Vijayasekaran Boovaragavan, Mounika Arabandi, Venkatasailanathan Ramadesigan, Venkat R Subramanian, Folarin Latinwo, and Richard D Braatz. "Optimal Spatial Distribution of Microstructure in Porous Electrodes for Li-ion Batteries." Proceedings of the 2010 American Control Conference.

[10]. Golmon, Stephanie, Kurt Maute, and Martin L. Dunn. "A Design Optimization Methodology for Li Batteries." Journal of Power Sources: 239-50.

[11]. Du, Wenbo, Amit Gupta, Xiangchun Zhang, Ann Marie Sastry, and Wei Shyy. "Effect of Cycling Rate, Particle Size and Transport Properties on Lithium-ion Cathode Performance." International Journal of Heat and Mass Transfer: 3552-561.

[12]. Golmon, Stephanie, Kurt Maute, and Martin L. Dunn. "Multiscale Design Optimization of Lithium Ion Batteries Using Adjoint Sensitivity Analysis." International Journal for Numerical Methods in Engineering Int. J. Numer. Meth. Engng, 2012, 475-94.

[13]. Stewart, Sarah G., Venkat Srinivasan, and John Newman. "Modeling the Performance of Lithium-Ion Batteries and Capacitors during Hybrid-Electric-Vehicle Operation." Journal of The Electrochemical Society J. Electrochem. Soc.

[14]. Caramia, Massimiliano, and Paolo Olmo. Multi-objective Management in Freight Logistics Increasing Capacity, Service Level and Safety with Optimization Algorithms. London: Springer, 2008.

[15]. Ngatchou, P., A. Zarei, and A. El-Sharkawi. "Pareto Multi Objective Optimization." Proceedings of the 13th International Conference On, Intelligent Systems Application to Power Systems.

[16]. Guo, Meng, Godfrey Sikha, and Ralph E. White. "Single-Particle Model for a Lithium-Ion Cell: Thermal Behavior." Journal of The Electrochemical Society J. Electrochem. Soc.

[17]. Lee, Kwang Y. Modern Heuristic Optimization Techniques Theory and Applications to Power Systems. Hoboken, N.J.: Wiley ;, 2008.

[18]. Deb, Kalyanmoy. Multi-objective Optimization Using Evolutionary Algorithms. Chichester: John Wiley & Sons, 2001.

[19]. Amouzgar, Kaveh. "Multi-objective optimization using Genetic Algorithms." (2012).

[20]. "Genetic Algorithm." - MATLAB. Accessed September 22, 2015.

[21]. "Documentation." Find Minima of Multiple Functions Using Genetic Algorithm. Accessed September 22, 2015.

[22]. "Documentation." Create Genetic Algorithm Options Structure. Accessed September 22, 2015.

[23]. Subramanian, V. R., et al. "Model reformulation and design of lithium ion batteries." Design for Energy and the Environment: Proceedings of the Seventh International Conference on Foundations of Computer-Aided Process Design. 2010.

[24]. Forman, Joel C., et al. "Genetic parameter identification of the doyle-fuller-newman model from experimental cycling of a lifepo 4 battery." Proceedings of the 2011 American Control Conference. IEEE, 2011.

[25]. Srinivasan, Venkat, and John Newman. "Discharge model for the lithium iron-phosphate electrode." Journal of the Electrochemical Society 151.10 (2004): A1517-A1529.

[26]. Thorat, Indrajeet V., et al. "Understanding rate-limiting mechanisms in LiFePO4 cathodes for Li-ion batteries." Journal of The Electrochemical Society 158.11 (2011): A1185-A1193.

[27]. Prada, Eric, et al. "Simplified electrochemical and thermal model of LiFePO4-graphite Li-ion batteries for fast charge applications." Journal of The Electrochemical Society 159.9 (2012): A1508-A1519.

[28]. Prada, Eric, et al. "A simplified electrochemical and thermal aging model of LiFePO4-graphite li-ion batteries: Power and capacity fade simulations."Journal of The Electrochemical Society 160.4 (2013): A616-A628.

[29]. Hong, Yao, and Cheol W. Lee. The Multiobjective Optimal Design Problems and their Pareto Optimal Fronts for Li-Ion Battery Cells. No. 2016-01-1199. SAE Technical Paper, 2016.

[30]. Lee, Cheol W., Yao Hong, Mushegh Hayrapetyan, and Zhimin Xi. "Systematic Derivation and Tuning of a Compact Differential-Algebraic Equations Model for LiFePO4-Graphite Li-Ion Batteries," To Appear in ECS Transactions, 2016.

Appendix I: Reaction Zone Model

The distance that the reaction zone has penetrated into the positive electrode (x_{rp}) and negative electrode (x_{rn}) depends on the amount of charge passed.

$$x_{rp} = \frac{it}{(1-\epsilon_+)q_+} \tag{A-1}$$

$$x_{rn} = \frac{it}{(1-\epsilon_-)q_-} \tag{A-2}$$

Where i is the discharging current density, t is the discharge time, ϵ_+ and ϵ_- are the porosity of two electrodes, q_+ and q_- are the capacity density of solids in the two electrodes (C/cm^3).

Thus, the voltage of the cell will be the open circuit potential minus the ohmic drop required for the ionic current to flow across the separator and through the pores in both electrodes between the narrow reaction zones.

$$V = U - i\left(\frac{L_s}{\kappa_s} + \frac{x_{rp}}{\kappa_+} + \frac{x_{rn}}{\kappa_-}\right) = U - \frac{L_s}{\kappa_s}i - \frac{i^2 t}{\kappa_+(1-\epsilon_+)q_+} - \frac{i^2 t}{\kappa_-(1-\epsilon_-)q_-} \tag{A-3}$$

Where the conductivity of the electrolyte phase is assumed to be given by the Bruggeman equation (A-4). κ_0 is the conductivity of the pore electrolyte when $\epsilon = 1$.

$$\kappa_i = \kappa_0 \epsilon_i^{1.5} \tag{A-4}$$

The energy (per unit area) for a constant discharge current density can be obtained with Equation A-5.

$$E = \int_0^{t_d} Vi\, dt = \left(U - \frac{L_s}{\kappa_s}i\right) it_d - \frac{i^3 t_d^2}{2\kappa_+(1-\epsilon_+)q_+} - \frac{i^3 t_d^2}{2\kappa_-(1-\epsilon_-)q_-} \tag{A-5}$$

For a same design and same discharging time, with different discharging current density, the energy (per unit area) is different. But for a given design, two constraints would exist for the discharge current density and thus limit the amount of energy delivered.

The first constraint is that the cell voltage needs to be larger than the cutoff voltage. The second constraint is the capacity of the positive electrode must not be exhausted as the capacity ratio between negative and positive electrodes is assumed to be greater than one.

$$U - \frac{L_s}{\kappa_s} i - \frac{i^2 t_d}{\kappa_+(1-\epsilon_+)q_+} - \frac{i^2 t_d}{\kappa_-(1-\epsilon_-)q_-} > V_C \qquad \text{(A-6)}$$

$$x_{rp} = \frac{i t_d}{(1-\epsilon_+)q_+} \leq L_+ \qquad \text{(A-7)}$$

i_{opt} is defined as the current density which could discharge the cell from the open circuit potential to the cutoff voltage exactly in the predetermined discharge time. Let $a = \frac{t_d}{\kappa_+(1-\epsilon_+)q_+} + \frac{t_d}{\kappa_-(1-\epsilon_-)q_-}$, $b = \frac{L_s}{\kappa_s}$ and $c = V_C - U$, the calculation of i_{opt} can be formulated by Equation (A-8)

$$i_{opt} = \min\left(\frac{-b+\sqrt{b^2-4ac}}{2a}, \frac{(1-\epsilon_+)q_+ L_+}{t_d}\right) \qquad \text{(A-8)}$$

The i_{opt} will be used to calculate the energy (per unit area) the cell could deliver for a discharging cycle with Equation A-5 since only with this current density the battery would stop working either because all the active materials are used up or the cell voltage is reduced to cutoff voltage.

Appendix II: Anticipated Shape of Pareto Front for The Two-Objective Optimization Problem

For each electrode porosity value ϵ_+,

$$\frac{dM}{dL_+} = [\rho_+(1-\epsilon_+) + \rho_e\epsilon_+] + [\rho_-(1-\epsilon_-) + \rho_e\epsilon_-] \cdot \frac{r(1-\epsilon_+)q_+}{(1-\epsilon_-)q_-} \tag{A-9}$$

$$\frac{d^2M}{dL_+^2} = 0 \tag{A-10}$$

So when L_+ increases, the unit area mass (M) of the cell will increase proportionally.

Consider the part where voltage constraint, which is given by Equation A-6 is not binding, the active materials in the positive electrode can be dried up after the discharging, then

$$i_{opt} = \frac{(1-\epsilon_+)q_+L_+}{t_d} \tag{A-11}$$

$$\frac{di_{opt}}{dL_+} = \frac{(1-\epsilon_+)q_+}{t_d} \tag{A-12}$$

$$\frac{d^2i_{opt}}{dL_+^2} = 0 \tag{A-13}$$

When L_+ increases, the optimal current density of discharging (i_{opt}) will increase proportionally.

On the other hand, the results of derivation calculations for unit area energy on discharging current density are given in Equation A-14 and Equation A-15

$$\frac{dE}{di} = Ut_d - \frac{2L_s}{\kappa_s}it_d - \frac{3i^2t_d^2}{2\kappa_+(1-\epsilon_+)q_+} - \frac{3i^2t_d^2}{2\kappa_-(1-\epsilon_-)q_-} \tag{A-14}$$

$$\frac{d^2E}{di^2} = \frac{2L_s}{\kappa_s}t_d - \frac{3it_d^2}{\kappa_+(1-\epsilon_+)q_+} - \frac{3it_d^2}{\kappa_-(1-\epsilon_-)q_-} < 0 \tag{A-15}$$

So, when i increases, the unit area Energy may firstly increase and then decrease. However, as we are only interested in the Pareto Front, only the increasing part will be discussed. As the second-order derivative is negative, when i increases, the unit area Energy will increase in a decelerating pace when discharging current density decreases.

According to the above discussion, we can imagine for a particular porosity value, the Pareto front will be a concave curve like shown in Figure A-1.

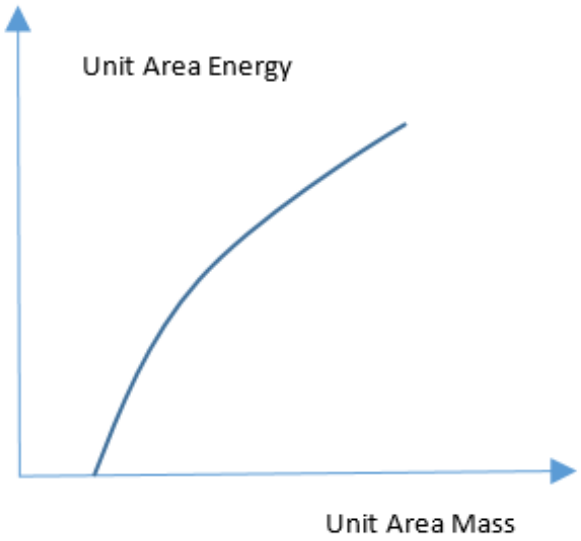

Figure A-1 Response Curve for a Particular ϵ_+

When the porosity of positive electrode is different, when the thickness of positive electrode is 0, the unit area mass will still be the unit area mass of separator and the remaining parts, which are assumed to be constant. So the starting point of the response curve will stay the same. And the shape of the curve will still be similarly concave, just with different curvature.

The overall Pareto front, therefore, is also a concave curve which could envelop all the response curves for different positive electrode porosity values, as shown with the red curve in Figure A-2.

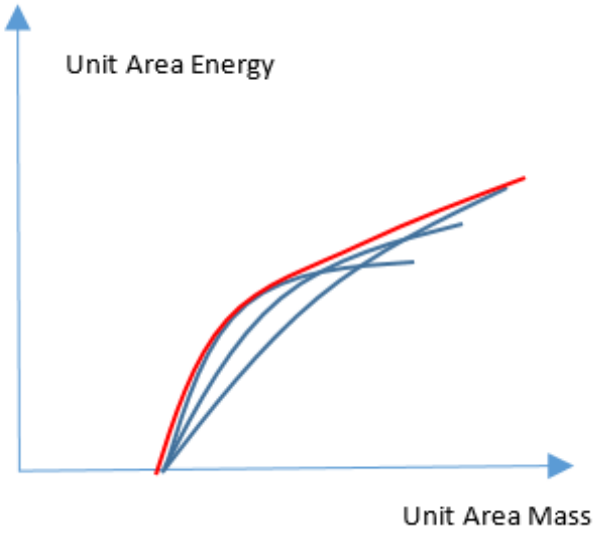

Figure A-2 Pareto Front and Response Curves for Different ϵ_+

Appendix III: The Effect of Increasing the Thickness of Electrodes on Energy is Capacity Limit

According to the reaction zone model, the distance that reaction zones penetrate into the two electrodes will be proportional, see Equation A-16.

$$x_{rn} = \frac{(1-\epsilon_+)q_+ x_{rp}}{(1-\epsilon_-)q_-} \tag{A-16}$$

Thus, the constraint of cutoff voltage can be written in Equation A-17.

$$U - \frac{iL_s}{\kappa_s} - i\left(\frac{1}{\kappa_+} + \frac{(1-\epsilon_+)q_+}{(1-\epsilon_-)q_-\kappa_-}\right)x_{rp} \geq V_c \tag{A-171}$$

When the thickness of positive electrode is small, for a predetermined discharging time, the discharging current density needs also to be small because of the lack of active materials for each unit area. Under such a circumstance, the voltage constraint is not binding. At the end of the discharging time, only the capacity constraint will be the real constraint limiting the performance of the battery. Thus, adding more active materials under this condition and make the cell a thicker one gives us a reasonable gain in the energy capacity because the new added active materials can be used up.

However, when the thickness of positive electrode exceeds some threshold value, the voltage constraint becomes binding due to greater i_{opt} and x_{rp}. After this point, adding more materials and making the cell thicker will not help a lot in delivering the energy. This is because the cell voltage will be reduced to the cutoff voltage before the active materials are used up in this case. For this case, adding more active materials for each unit area and have thicker

electrodes only increase the amount of unusable active materials for the discharging cycles and will not give significant improvement in the energy capacity to the cell.

Thus, for a large target energy capacity, the contribution of making the electrodes thicker is limited by some boundary values, a larger separator area will be needed to obtain such a high energy requirement.